Shear viscosity for finitely extensible chains with fluctuating internal friction and hydrodynamic interactions

R. Kailasham,[1, a)] Rajarshi Chakrabarti,[2, b)] and J. Ravi Prakash[3, c)]
[1)] *Department of Chemical Engineering, Carnegie Mellon University, Pittsburgh, Pennsylvania - 15232, USA*
[2)] *Department of Chemistry, Indian Institute of Technology Bombay, Mumbai, Maharashtra - 400076, India*
[3)] *Department of Chemical Engineering, Monash University, Melbourne, VIC 3800, Australia*

An exact solution of coarse-grained polymer models with fluctuating internal friction and hydrodynamic interactions has not been proposed so far due to a one-to-all coupling between the connector vector velocities that precludes the formulation of the governing stochastic differential equations. A methodology for the removal of this coupling is presented, and the governing stochastic differential equations, obtained by attaching a kinetic interpretation to the Fokker-Planck equation for the system, are integrated numerically using Brownian dynamics simulations. The proposed computational route eliminates the calculation of the divergence of the diffusion tensor which appears in models with internal friction, and is about an order of magnitude faster than the recursion-based decoupling algorithm previously developed [J. Rheol. **65**, 903 (2021)] for the solution of freely draining models with internal friction. The effects of the interplay of various combinations of finite extensibility, internal friction and hydrodynamic interactions on the steady-shear-viscosity is examined. While finite extensibility leads solely to shear-thinning, both internal friction and hydrodynamic interactions result in shear-thinning followed by shear-thickening. The shear-thickening induced by internal friction effects are more pronounced than that due to hydrodynamic interactions.

arXiv:2204.10656v1 [cond-mat.soft] 22 Apr 2022

I. INTRODUCTION

The time rate of spatial reorganization in polymer molecules is modulated both by solvent drag, and solvent-viscosity-independent intramolecular interactions, collectively termed as "internal friction" or "internal viscosity" (IV). For example, the timescale of protein folding and reconfiguration[1–5], the mechanical response of polysaccharides[6] and collapsed DNA globules[7] to force spectroscopy, and the coil-stretch transition of polymer chains in turbulent flow[8], have all been shown to be affected by the presence of IV. Parallelly, the importance of accounting for solvent-mediated momentum transfer between polymer chain segments, also known as hydrodynamic interactions (HI), on the dynamics of macromolecules is also well-documented[9–12]. An exact solution to coarse-grained polymer models with arbitrary degrees of freedom that incorporate both IV and HI effects has so far remained elusive. In this paper, we present the derivation of the governing stochastic differential equations for such a model, outline an algorithm for its exact solution, derive a thermodynamically consistent stress tensor expression for this model, and use it to predict the steady-shear viscosity of polymer chain models with fluctuating internal friction and hydrodynamic interactions using Brownian dynamics (BD) simulations.

Polymer chains are capable of being stretched and reoriented, undergoing configurational changes both at equilibrium (representing the chain suspended in a quiescent fluid) and in the presence of a flow field. These macromolecules are routinely modeled[13] as a linear sequence of massless beads connected by springs, where the former represent centres of friction, and the latter model the entropic elasticity of the polymer chain. The Rouse model for polymers, which consists of beads connected by Hookean springs, is solvable analytically, and predicts a non-zero value for the first normal stress difference observed in non-Newtonian polymer solutions. This rudimentary model, however, fails to predict the shear-thinning of viscosity in dilute polymer solutions. Additional constraints and mechanisms, such as the finite extensibility (FE) of the chain, the solvent-mediated transfer of momentum between chain segments, also referred to as hydrodynamic interactions (HI), and the solvent quality, have been cited and invoked in attempts to build more accurate polymer models[13–15]. The inclusion of such non-linear effects into the standard bead-spring-chain framework, however, renders an analytical solution intractable, and necessitates the use of numerical methods for its solution. Using BD simulations, it has been possible by incorporating these molecular scale phenomena, to obtain a quantitative, parameter-free agreement between computational predictions and experimental observations for the extension of DNA solutions in elongational flow[16–19]. None of the nonlinear effects mentioned above, however, can explain the discontinuous jump in stress of polymer solutions at the inception of flow (termed "stress jump")[20,21], which is hypothesized to originate from the frictional resistance offered by the polymer chain to short-time-scale variations in its conformation[22–25].

The energy difference between the *trans* and *gauche* conformations determines the static flexibility, or persistence length of polymers[26]. The activation barrier separating these two states, represents the resistance to dihedral angle rotations, and determines the timescale be-

[a)] Electronic mail: rkailash@andrew.cmu.edu
[b)] Electronic mail: rajarshi@chem.iitb.ac.in
[c)] Electronic mail: ravi.jagadeeshan@monash.edu

low which the molecule appears rigid and resists changes to its configuration[27,28]. This resistance to dihedral angle rotations had been suspected, since the inception of polymer kinetic theory, to be a source of internal friction[22]. Molecular dynamics simulations[29,30] and recent experiments on intrinsically disordered proteins[5] appear to confirm this notion. This rate-dependent force that resists relative motion between chain segments is incorporated into the bead-spring-chain model by the addition of viscous dashpots[22,24,31–33] or dampers in parallel with the springs. The inclusion of dashpots, however, results in a coupling of the velocities of the connector vectors that join adjacent beads, rendering an exact solution infeasible for all but the simplest case of a dumbbell model[32,34,35] (two beads connected by a spring). Such a coupling precludes both the formulation of a Fokker-Planck equation for the configurational distribution function of the chain, and by extension, the derivation of the stochastic differential equations governing the motion of beads.

Manke and Williams [24] derived a semi-analytical approximation for the stress jump of free-draining bead-spring-dashpots, using a recursive-algorithm for the decoupling of bead velocities, leveraging the fact that in the absence of HI only the velocities of nearest neighbors in the chain are coupled, and restricted their analysis to the linear viscoelastic regime. In a prior work[36], we used the decoupling methodology developed by Manke and Williams [24] to derive and solve the exact set of stochastic differential equations governing the motion of free-draining bead-spring-dashpot chains that is valid both at equilibrium and in the presence of flow. By comparison against BD simulation results, it was established that the Manke and Williams [24] prediction for the stress jump improves with the number of beads in the chain. The framework developed by Manke and Williams[24,37,38] is applicable, however, only for linear viscoelastic predictions, and numerical simulations are required, as explained in ref. 36, for the calculation of viscometric functions in the presence of a flow field.

The exact formulation and solution of free-draining bead-spring-dashpot chains permitted an investigation[39] of the Rouse model with internal friction[6,40] (RIF), a widely used theoretical framework for the interpretation of internal friction effects in biophysical contexts which relies on a preaveraged treatment of internal friction. While the RIF model predicts that the relaxation time of the end-to-end vector in a chain diverges in the asymptotic limit of infinite IV, the incorporation of fluctuations in the IV force results, more realistically, in a finite value for the relaxation time under the same limit. Furthermore, the viscosity of the preaveraged model is found to be independent of the shear rate, while the exact model predicts a shear-rate dependent viscosity that undergoes both thinning and thickening. Additionally, the importance of accounting for fluctuations in HI for the estimation of viscometric functions is now well-understood[41–43].

The simultaneous inclusion of fluctuating internal friction and hydrodynamic interaction effects, however, results in a one-to-all coupling of the connector vector velocities, which does not permit the use of the decoupling approach developed previously for free-draining models with internal friction. Fixman remarked[44] that the solution of such a model would require "complicated matrix operations that may well be impractical unless preaveraging of the matrices is introduced." Using a preaveraged version of the hydrodynamic interaction tensor, Manke and Williams [37] applied the decoupling algorithm to solve for the stress jump of such chains in planar and elongational flow, and also derived semi-analytical results for material functions in small amplitude oscillatory shear flow[38]. The accuracy of these approximate results have remained untested from a theoretical standpoint, due to the unavailability of exact solutions to the bead-spring-dashpot chain model with fluctuating hydrodynamic interactions. In this paper, we prescribe an exact solution methodology for this model, and present preliminary rheological results. The present algorithm may also be applied to the free-draining IV model and is found to be an order of magnitude faster than the decoupling-methodology-based implementation developed recently[36].

A distinguishing feature of models with internal friction is the appearance of the divergence of the diffusion tensor in the governing stochastic differential equation obtained from an Itô interpretation of the underlying Fokker-Planck equation. The assumed incompressibility of the solvent ensures that this divergence is zero for polymer models with hydrodynamic interactions in an unbounded geometry[45], but this simplification does not hold when IV is included. Hütter and Öttinger [46] prescribe a numerical algorithm for the solution of such stochastic differential equations that relies on the kinetic interpretation[47–49] of the governing Fokker-Planck equation. This route replaces the calculation of the divergence of the diffusion tensor by that of its inverse, and has been recommended as being numerically more efficient except for cases in which a closed-form expression for the divergence is available. This approach has been used predominantly in simulations of colloidal particles and suspensions[50–52], and polymer chain models with constraints[53], such as the bead-rod-model. We show that the coupling of connector vector velocities in our model may be removed by the use of simple linear algebra, and employ the technique suggested by Hütter and Öttinger [46] for the numerical integration of the resulting stochastic differential equations.

While the time-evolution of the configuration of a polymer chain model with fluctuating IV and HI may be obtained from simulations without explicit calculation of the divergence of the diffusion tensor, the thermodynamically consistent stress tensor expression for this model, however, contains the divergence term. We employ the random finite difference (RFD) algorithm, developed by Donev and coworkers[54,55] for the calculation of this divergence term. We discuss later in Sec. II, why nevertheless,

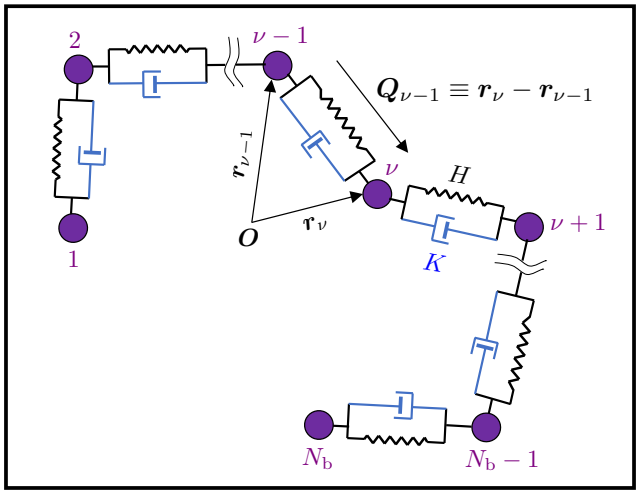

FIG. 1. Micromechanical model for a polymer chain, consisting of a sequence of beads connected by spring-dashpots. Each spring is associated with a Hookean spring constant H, and the damping coefficient of each dashpot is K.

the kinetic interpretation is still preferable to evaluating the divergence term, while solving the governing stochastic differential equation.

The most iconic rheological characteristic of dilute polymer solutions, namely, the shear-thinning of viscosity, has been attributed to several nonlinear intramolecular effects, including but not limited to: finite extensibility of the polymer chain, excluded volume effects[14,15] (EV), hydrodynamic interactions[56,57], and internal friction. Preliminary investigations of the steady-shear rheology of bead-spring-dashpot models relied on a Gaussian approximation of IV[58–60], predicting a shear-thinning of viscosity following a constant Newtonian plateau. Subsequent (exact) BD simulations[32,34–36] established that internal friction causes shear-thinning at low-to-moderate shear rates, followed by a thickening of the viscosity at higher shear rates. Finite extensibility is known to exclusively induce shear-thinning[13], while the inclusion of hydrodynamic interactions in coarse-grained models with greater than six beads has been shown to result in shear-thinning followed by thickening[42,43,61]. In this paper, we use an exact model that accounts for fluctuations in internal viscosity and hydrodynamic interactions, to systematically disentangle the impact of FE, IV, and HI on the steady-shear viscosity profile of bead-spring-dashpot chains.

The rest of the paper is structured as follows. Sec. II describes the bead-spring-dashpot chain model for a polymer, presents the governing stochastic differential equations and the stress tensor expression, and outlines simulation details pertaining to the numerical integration of the governing equations. Sec. III, which is a compilation of our results and the relevant discussion, is divided into three sections; Sec. III A deals with code validation, Sec. III B presents results for the stress jump at the inception of shear flow, and Sec. III C contains results for steady shear viscometric functions. We conclude in Sec. IV. Additional details pertaining to the study are presented in the Supplementary Material. Section SII of the Supplementary Material establishes that the Fokker-Planck equation for a dumbbell, with fluctuating IV and HI derived using the methodology developed in the present work, corresponds to that obtained previously by an alternative route in ref. 35. In Sec. SIII, the symmetricity and positive-definiteness of the diffusion tensor for the present model is illustrated empirically. Sec. SIV establishes the equivalence between the present methodology and the decoupling algorithm developed in ref. 36 for free-draining bead-spring-dashpot chains, and also compares the computational cost for the two approaches. Sec. SV illustrates that the governing equations for the present model satisfy the fluctuation dissipation theorem, and the time-step convergence of the BD simulation results presented in this work is established in Sec. SVI. Lastly, Sec. SVII of the Supplementary Material contains the detailed steps for the derivation of the stress tensor expression used in the evaluation of shear viscosity from BD simulations.

II. GOVERNING EQUATION AND SIMULATION DETAILS

We consider a micromechanical model for a linear polymer chain that consists of N_b massless beads, each of radius a, joined by $N \equiv (N_\mathrm{b}-1)$ springs. The Hookean spring constant associated with each spring is H, and the dashpot in parallel with each spring has a damping coefficient of K, as shown in Fig. 1. The position of the i^th bead is denoted as $\boldsymbol{r}_i$, and the connector vector joining adjacent beads is represented as $\boldsymbol{Q}_{i-1} \equiv \boldsymbol{r}_i - \boldsymbol{r}_{i-1}$. The chain, as shown in Fig. 1, is suspended in a Newtonian solvent of viscosity η_s where the velocity $\boldsymbol{v}_\mathrm{f}$ at any location $\boldsymbol{r}_\mathrm{f}$ in the fluid is given by $\boldsymbol{v}_\mathrm{f}(\boldsymbol{r}_\mathrm{f},t) \equiv \boldsymbol{v}_0 + \boldsymbol{\kappa}(t)\cdot\boldsymbol{r}_\mathrm{f}$, where $\boldsymbol{v}_0$ is a constant vector, and the transpose of the velocity gradient tensor is denoted as $\boldsymbol{\kappa} \equiv (\nabla \boldsymbol{v}_\mathrm{f})^T$. The chain is assumed to have equilibrated in momentum space, and its normalized configurational distribution function at any time t is given by $\Psi \equiv \Psi(\boldsymbol{r}_1,\boldsymbol{r}_2,...,\boldsymbol{r}_{N_\mathrm{b}},t) = (1/\mathcal{Z})\exp[-\phi/k_BT]$, where ϕ represents the intramolecular potential energy stored in the springs joining the beads, k_B is Boltzmann's constant, T the absolute temperature, and the partition function $\mathcal{Z} = \int \exp[-\phi/k_BT]\, d\boldsymbol{Q}_1 d\boldsymbol{Q}_2 \ldots d\boldsymbol{Q}_N$. The spring force in the k^th connector vector is denoted as $\boldsymbol{F}_k^{(\mathrm{c})} = \partial\phi/\partial\boldsymbol{Q}_k$. Both Hookean and finitely extensible nonlinear elastic (FENE) springs are considered in this work, and the functional form of these spring force laws are provided below. The expression for the internal viscosity force, $\boldsymbol{F}_k^\mathrm{IV}$, in the k^th connector vector may be written as $\boldsymbol{F}_k^\mathrm{IV} = K\left(\boldsymbol{Q}_k\boldsymbol{Q}_k/Q_k^2\right)\cdot[\![\dot{\boldsymbol{Q}}_k]\!]$, where $[\![\ldots]\!]$ denotes an average over momentum-space. Within the framework of polymer kinetic theory[13], the Fokker-Planck equation for the configurational distribution func-

tion is obtained by combining a force-balance on the beads (or connector vectors) with a continuity equation in probability space. The force-balance dictates that the sum of the restoring force from the spring, the internal friction force due to the dashpot, the random Brownian force arising from collisions with solvent molecules, and the hydrodynamic force which represents the solvent's resistance to the motion of the bead, equals zero. The friction coefficient associated with each bead is given by $\zeta = 6\pi\eta_{\rm s}\,a$, and is used to define the timescale for the model, $\lambda_H = \zeta/4H$. The length-scale is taken to be $l_H = \sqrt{k_BT/H}$. Dimensionless quantities are denoted with an asterisk as superscript, for example, $a^* = a/l_H$.

In the following derivation, summations are indicated explicitly, and the Einstein convention is not adopted. For a chain with N springs, the following equations of motion for the velocity of the connector vector and the centre of mass has been derived in Ref. 33,

$$[\![\dot{\boldsymbol{Q}}_j]\!] = \boldsymbol{\kappa}\cdot\boldsymbol{Q}_j - \frac{1}{\zeta}\sum_{k=1}^{N}\tilde{\boldsymbol{A}}_{jk}\cdot\left(k_BT\frac{\partial\ln\Psi}{\partial\boldsymbol{Q}_k} + \frac{\partial\phi}{\partial\boldsymbol{Q}_k} + K\frac{\boldsymbol{Q}_k\boldsymbol{Q}_k}{\boldsymbol{Q}_k^2}\cdot[\![\dot{\boldsymbol{Q}}_k]\!]\right) \tag{1}$$

$$[\![\dot{\boldsymbol{r}}_{\rm c}]\!] = \boldsymbol{v}_o + \boldsymbol{\kappa}\cdot\boldsymbol{r}_{\rm c} - \frac{1}{N_{\rm b}\zeta}\sum_{\mu,\nu=1}^{N_{\rm b}}\sum_{k=1}^{N}\bar{B}_{k\mu}\left(\delta_{\mu\nu}\boldsymbol{\delta} + \zeta\boldsymbol{\Omega}_{\mu\nu}\right)\cdot\left(k_BT\frac{\partial\ln\Psi}{\partial\boldsymbol{Q}_k} + \frac{\partial\phi}{\partial\boldsymbol{Q}_k} + K\frac{\boldsymbol{Q}_k\boldsymbol{Q}_k}{\boldsymbol{Q}_k^2}\cdot[\![\dot{\boldsymbol{Q}}_k]\!]\right) \tag{2}$$

where

$$\tilde{\boldsymbol{A}}_{jk} = A_{jk}\boldsymbol{\delta} + \zeta\left(\boldsymbol{\Omega}_{j,k} + \boldsymbol{\Omega}_{j+1,k+1} - \boldsymbol{\Omega}_{j,k+1} - \boldsymbol{\Omega}_{j+1,k}\right) \tag{3}$$

$$\bar{B}_{k\mu} = \delta_{k+1,\mu} - \delta_{k\mu} \tag{4}$$

and A_{jk} are the elements of the Rouse matrix, given as

$$A_{jk} = \begin{cases} 2; & j = k \\ -1; & |j-k| = 1 \\ 0; & \text{otherwise} \end{cases} \tag{5}$$

The general form of the symmetric hydrodynamic interaction tensor, $\boldsymbol{\Omega}_{\mu\nu}$, is given by

$$\boldsymbol{\Omega}_{\mu\nu} = \frac{3a}{4\zeta\,r_{\mu\nu}}\left\{\mathscr{A}\boldsymbol{\delta} + \mathscr{B}\frac{\boldsymbol{r}_{\mu\nu}\boldsymbol{r}_{\mu\nu}}{\boldsymbol{r}_{\mu\nu}^2}\right\} \tag{6}$$

with $\boldsymbol{r}_{\mu\nu} = \boldsymbol{r}_\nu - \boldsymbol{r}_\mu$ denoting the interbead separation and the coefficients $\mathscr{A}$ and $\mathscr{B}$, according to the Rotne-Prager-Yamakawa (RPY) definition[62,63], are given by

$$\begin{aligned} \mathscr{A} &= \left(1 + \frac{2a^2}{3r_{\mu\nu}^2}\right), \quad \mathscr{B} = \left(1 - \frac{2a^2}{r_{\mu\nu}^2}\right) \quad \text{for} \quad r_{\mu\nu} \geq 2a \\ \mathscr{A} &= \frac{r_{\mu\nu}}{2a}\left(\frac{8}{3} - \frac{3r_{\mu\nu}}{4a}\right), \quad \mathscr{B} = \frac{1}{8}\left(\frac{r_{\mu\nu}}{a}\right)^2 \quad \text{for} \quad r_{\mu\nu} < 2a \end{aligned} \tag{7}$$

where the hydrodynamic interaction parameter is defined to be, $h^* = a^*/\sqrt{\pi}$, with $h^* = 0$ denoting the free-draining case. Self-interactions are suppressed by requiring that $\boldsymbol{\Omega}_{\mu\nu} = \boldsymbol{0}$ for $\mu = \nu$. Defining $\varphi = (K/\zeta)$, Eq. (1) yields, upon simplification,

$$[\![\dot{\boldsymbol{Q}}_j]\!] = \boldsymbol{\kappa}\cdot\boldsymbol{Q}_j - \frac{1}{\zeta}\sum_{k=1}^{N}\tilde{\boldsymbol{A}}_{jk}\cdot\left(k_BT\frac{\partial\ln\Psi}{\partial\boldsymbol{Q}_k} + \frac{\partial\phi}{\partial\boldsymbol{Q}_k}\right) - \varphi\sum_{k=1}^{N}\tilde{\boldsymbol{Z}}_{jk}\cdot[\![\dot{\boldsymbol{Q}}_k]\!] \tag{8}$$

where

$$\tilde{\boldsymbol{Z}}_{jk} = \tilde{\boldsymbol{A}}_{jk}\cdot\left(\frac{\boldsymbol{Q}_k\boldsymbol{Q}_k}{\boldsymbol{Q}_k^2}\right) \tag{9}$$

Further analysis is simplified if the $k = j$ and the $k \neq j$ cases in the last term on the RHS of Eq. (8) are treated separately

$$[\![\dot{\boldsymbol{Q}}_j]\!] = \boldsymbol{\kappa} \cdot \boldsymbol{Q}_j - \frac{1}{\zeta} \sum_{k=1}^{N} \tilde{\boldsymbol{A}}_{jk} \cdot \left(k_B T \frac{\partial \ln \Psi}{\partial \boldsymbol{Q}_k} + \frac{\partial \phi}{\partial \boldsymbol{Q}_k} \right) - \varphi \tilde{\boldsymbol{Z}}_{jj} \cdot [\![\dot{\boldsymbol{Q}}_j]\!] - \varphi \sum_{k \neq j}^{N} \tilde{\boldsymbol{Z}}_{jk} \cdot [\![\dot{\boldsymbol{Q}}_k]\!] \tag{10}$$

Grouping the terms containing $[\![\dot{\boldsymbol{Q}}_j]\!]$ and simplifying,

$$[\![\dot{\boldsymbol{Q}}_j]\!] = \boldsymbol{Y}_{jj} \cdot (\boldsymbol{\kappa} \cdot \boldsymbol{Q}_j) - \frac{1}{\zeta} \sum_{k=1}^{N} \left(\boldsymbol{Y}_{jj} \cdot \tilde{\boldsymbol{A}}_{jk} \right) \cdot \left(k_B T \frac{\partial \ln \Psi}{\partial \boldsymbol{Q}_k} + \frac{\partial \phi}{\partial \boldsymbol{Q}_k} \right) - \varphi \sum_{k \neq j}^{N} \left(\boldsymbol{Y}_{jj} \cdot \tilde{\boldsymbol{Z}}_{jk} \right) \cdot [\![\dot{\boldsymbol{Q}}_k]\!] \tag{11}$$

where

$$\boldsymbol{Y}_{jj} = \left(\boldsymbol{\delta} + \varphi \tilde{\boldsymbol{Z}}_{jj} \right)^{-1} \tag{12}$$

$$\tilde{\boldsymbol{Z}}_{jj} = 2 \left(\boldsymbol{\delta} - \zeta \boldsymbol{\Omega}_{j,j+1} \right) \cdot \left(\frac{\boldsymbol{Q}_j \boldsymbol{Q}_j}{\boldsymbol{Q}_j^2} \right) = 2 \beta_j \left(\frac{\boldsymbol{Q}_j \boldsymbol{Q}_j}{\boldsymbol{Q}_j^2} \right) \tag{13}$$

with

$$\beta_j = \left[1 - \frac{3a}{4Q_j} \left(\mathscr{A} + \mathscr{B} \right) \right] \tag{14}$$

Using Eqs. (13) and (14), Eq. (12) is simplified to give

$$\boldsymbol{Y}_{jj} = \left[\boldsymbol{\delta} + \epsilon \beta_j \left(\frac{\boldsymbol{Q}_j \boldsymbol{Q}_j}{\boldsymbol{Q}_j^2} \right) \right]^{-1} = \left[\boldsymbol{\delta} - \frac{\epsilon \beta_j}{\epsilon \beta_j + 1} \frac{\boldsymbol{Q}_j \boldsymbol{Q}_j}{\boldsymbol{Q}_j^2} \right] \tag{15}$$

where $\epsilon = 2\varphi$, and the inverse has been obtained analytically using the Sherman-Morrison theorem[64], as described in Ref. 35. We may further rewrite Eq. (11) as

$$\sum_{k=1}^{N} \boldsymbol{J}_{jk} \cdot [\![\dot{\boldsymbol{Q}}_k]\!] = \boldsymbol{Y}_{jj} \cdot (\boldsymbol{\kappa} \cdot \boldsymbol{Q}_j) - \frac{1}{\zeta} \sum_{k=1}^{N} \boldsymbol{X}_{jk} \cdot \left(k_B T \frac{\partial \ln \Psi}{\partial \boldsymbol{Q}_k} + \frac{\partial \phi}{\partial \boldsymbol{Q}_k} \right) \tag{16}$$

with

$$\boldsymbol{X}_{jk} = \boldsymbol{Y}_{jj} \cdot \tilde{\boldsymbol{A}}_{jk} \tag{17}$$

and

$$\boldsymbol{J}_{jk} = \begin{cases} \boldsymbol{\delta}; & j = k \\ \\ \varphi \boldsymbol{Y}_{jj} \cdot \tilde{\boldsymbol{Z}}_{jk}; & j \neq k \end{cases} \tag{18}$$

We define the collective coordinates

$$\begin{aligned} \boldsymbol{\mathcal{Q}} &\equiv [\boldsymbol{Q}_1, \boldsymbol{Q}_2, ..., \boldsymbol{Q}_N] \\ &\equiv \left[Q_1^1, Q_1^2, Q_1^3, Q_2^1, Q_2^2, ..., Q_N^3 \right] \end{aligned} \tag{19}$$

and write $\mathcal{Q}_i = Q_j^\omega$, where $j = 1, 2, ..., N$ and $\omega = 1, 2, 3$ represent Cartesian components in the x, y, z directions, respectively, with i related to j and ω as $i = 3(j-1) + \omega$. Similarly, $\boldsymbol{\mathcal{F}}^\phi \equiv \left[\boldsymbol{F}_1^\phi, \boldsymbol{F}_2^\phi, ..., \boldsymbol{F}_N^\phi \right]$, with $\boldsymbol{F}_j^\phi = (\partial \phi / \partial \boldsymbol{Q}_j)$. We next define the dimensionless block matrices $\boldsymbol{\mathcal{Y}}$, $\boldsymbol{\mathcal{X}}$, and $\boldsymbol{\mathcal{J}}$, each of size $N \times N$, and whose elements are the 3×3 matrices given by Eqs. (15), (17), and (18), respectively. Note that the diagonal elements of $\boldsymbol{\mathcal{Y}}$ and $\boldsymbol{\mathcal{K}}$ are given by Eq. (15) and $\boldsymbol{\kappa}$, respectively, with their off-diagonal elements set to $\boldsymbol{0}$.

In terms of collective coordinates, we define

$$\boldsymbol{\mathcal{M}} = \boldsymbol{\mathcal{J}}^{-1} \cdot \boldsymbol{\mathcal{Y}} \tag{20}$$

$$\boldsymbol{\mathcal{D}} = \frac{1}{2}\left(\boldsymbol{\mathcal{J}}^{-1} \cdot \boldsymbol{\mathcal{X}}\right) \tag{21}$$

and rewrite Eq. (16) as

$$[\![\dot{\boldsymbol{\mathcal{Q}}}]\!] = \boldsymbol{\mathcal{M}} \cdot (\boldsymbol{\mathcal{K}} \cdot \boldsymbol{\mathcal{Q}}) - \frac{2k_BT}{\zeta}\underline{\boldsymbol{\mathcal{D}} \cdot \left(\frac{\partial \ln \Psi}{\partial \boldsymbol{\mathcal{Q}}}\right)} - \frac{2}{\zeta}\boldsymbol{\mathcal{D}} \cdot \boldsymbol{\mathcal{F}}^{\phi} \tag{22}$$

which represents a fully decoupled expression for $[\![\dot{\boldsymbol{\mathcal{Q}}}]\!]$ that may be substituted into the equation of continuity. Eq. (22) is rewritten in terms of the individual connector vectors as follows

$$[\![\dot{\boldsymbol{Q}}_j]\!] = \sum_{k=1}^{N} \boldsymbol{M}_{jk} \cdot (\boldsymbol{\kappa} \cdot \boldsymbol{Q}_k) - \frac{2k_BT}{\zeta}\sum_{k=1}^{N} \boldsymbol{D}_{jk} \cdot \left(\frac{\partial \ln \Psi}{\partial \boldsymbol{Q}_k}\right) - \frac{2}{\zeta}\sum_{k=1}^{N} \boldsymbol{D}_{jk} \cdot \left(\frac{\partial \phi}{\partial \boldsymbol{Q}_k}\right) \tag{23}$$

where $\boldsymbol{M}_{jk}$ and $\boldsymbol{D}_{jk}$ are 3×3 matrices which are elements of $\boldsymbol{\mathcal{M}}$ and $\boldsymbol{\mathcal{D}}$, respectively. The j^{th} element of the underlined term in Eq. (22) is to be interpreted as

$$\left[\boldsymbol{\mathcal{D}} \cdot \left(\frac{\partial \ln \Psi}{\partial \boldsymbol{\mathcal{Q}}}\right)\right]_j = \sum_{k=1}^{N} \boldsymbol{D}_{jk} \cdot \left(\frac{\partial \ln \Psi}{\partial \boldsymbol{Q}_k}\right) \tag{24}$$

Substituting Eq. (23) into the equation of continuity,

$$\frac{\partial \Psi}{\partial t} = -\sum_{j=1}^{N} \frac{\partial}{\partial \boldsymbol{Q}_j} \cdot \left\{[\![\dot{\boldsymbol{Q}}_j]\!]\Psi\right\}, \tag{25}$$

the Fokker-Planck equation is obtained as

$$\frac{\partial \Psi}{\partial t} = -\sum_{j=1}^{N} \frac{\partial}{\partial \boldsymbol{Q}_j} \cdot \left\{\left[\sum_{k=1}^{N} \boldsymbol{M}_{jk} \cdot (\boldsymbol{\kappa} \cdot \boldsymbol{Q}_k) - \frac{2}{\zeta}\sum_{k=1}^{N} \boldsymbol{D}_{jk} \cdot \left(\frac{\partial \phi}{\partial \boldsymbol{Q}_k}\right)\right]\Psi\right\} + \left(\frac{2k_BT}{\zeta}\right)\sum_{j,k=1}^{N} \frac{\partial}{\partial \boldsymbol{Q}_j} \cdot \boldsymbol{D}_{jk} \cdot \frac{\partial \Psi}{\partial \boldsymbol{Q}_k} \tag{26}$$

It is observed empirically that $\boldsymbol{D}_{jk}^T = \boldsymbol{D}_{kj}$, resulting in $\boldsymbol{\mathcal{D}} = \boldsymbol{\mathcal{D}}^T$, and the symmetricity and positive-definiteness of $\boldsymbol{\mathcal{D}}$ are discussed in detail in Sec. SIII of the Supplementary Material. The second term on the RHS of Eq. (26) must be processed further in order to cast the Fokker-Planck equation in a form amenable to the Itô interpretation. Following the procedure outlined in Ref. 36, the dimensionless governing Fokker-Planck equation is obtained as

$$\begin{aligned}\frac{\partial \Psi^*}{\partial t^*} = -\sum_{j=1}^{N} \frac{\partial}{\partial \boldsymbol{Q}_j^*} \cdot \Bigg\{\Bigg[&\sum_{k=1}^{N} \boldsymbol{M}_{jk} \cdot (\boldsymbol{\kappa}^* \cdot \boldsymbol{Q}_k^*) - \frac{1}{2}\sum_{k=1}^{N} \boldsymbol{D}_{jk} \cdot \left(\frac{\partial \phi^*}{\partial \boldsymbol{Q}_k^*}\right) \\ &+ \frac{1}{2}\sum_{k=1}^{N} \frac{\partial}{\partial \boldsymbol{Q}_k^*} \cdot \boldsymbol{D}_{jk}^T\Bigg]\Psi^*\Bigg\} + \frac{1}{2}\sum_{j,k=1}^{N} \frac{\partial}{\partial \boldsymbol{Q}_j^*}\frac{\partial}{\partial \boldsymbol{Q}_k^*} : \left[\boldsymbol{D}_{jk}^T\Psi^*\right]\end{aligned} \tag{27}$$

where

$$\Psi^* = \Psi l_H^3,\ t^* = t/\lambda_H,\ \phi^* = \phi/k_BT, \quad \text{and} \quad \boldsymbol{Q}_j^* = \boldsymbol{Q}_j/l_H. \tag{28}$$

Setting $N = 1$ in eq. (27), followed by simplification, yields the previously derived[35] governing Fokker-Planck equation for a dumbbell with fluctuating IV and HI, as shown in Sec. SII of the Supplementary Material.

The dimensionless form of the force in a connector vector k corresponding to the two types of springs considered in this work is given as follows:

$$\boldsymbol{F}_k^{*(\mathrm{c})} = \begin{cases} \boldsymbol{Q}_k^*; & \text{Hookean} \\ \dfrac{\boldsymbol{Q}_k^*}{1 - Q_k^{*2}/b}; & \text{FENE} \end{cases} \tag{29}$$

The parameter b denotes the square of the maximum permissible stretch of the spring in dimensionless units, and its value for a given polymer may be found from its experimentally measured radius of gyration under θ-solvent conditions, and its contour length[16]. We do not seek to model a specific polymer in this work, and use $b = 100$ in all our simulations that employ FENE springs. The use of this value of b appears to be prevalent in computational rheological studies[32,65,66].

The stochastic differential equation corresponding to Eq. (27) under the Itô interpretation may be written in terms of collective coordinates to be

$$d\boldsymbol{\mathcal{Q}}^* = \left[\boldsymbol{\mathcal{A}}^*(\boldsymbol{\mathcal{Q}}^*) + \frac{1}{2}\boldsymbol{\nabla}^* \cdot \boldsymbol{\mathcal{D}}\right] dt^* + \boldsymbol{\mathcal{B}} \cdot\, d\boldsymbol{\mathcal{W}}^* \tag{30}$$

where

$$\boldsymbol{\mathcal{A}}^*(\boldsymbol{\mathcal{Q}}^*) = \boldsymbol{\mathcal{M}} \cdot (\boldsymbol{\mathcal{K}}^* \cdot \boldsymbol{\mathcal{Q}}^*) - \frac{1}{2}\boldsymbol{\mathcal{D}} \cdot \boldsymbol{\mathcal{F}}^{*\phi} \tag{31}$$

$$\boldsymbol{\mathcal{B}} \cdot \boldsymbol{\mathcal{B}}^T = \boldsymbol{\mathcal{D}} \tag{32}$$

and $\boldsymbol{\mathcal{W}}^*$ is a $3N$-dimensional Wiener process. The j^{th} element of $(\boldsymbol{\nabla}^* \cdot \boldsymbol{\mathcal{D}})$ is the three-component vector denoted by

$$(\boldsymbol{\nabla}^* \cdot \boldsymbol{\mathcal{D}})_j = \sum_{k=1}^{N} \frac{\partial}{\partial \boldsymbol{Q}_k^*} \cdot \boldsymbol{D}_{kj} \tag{33}$$

While there exist infinitely many choices for the block matrix $\boldsymbol{\mathcal{B}}$ that satisfies the fluctuation-dissipation theorem given in eq. (32), we set it to be the square root of the block diffusion tensor, $\boldsymbol{\mathcal{B}} = \boldsymbol{\mathcal{D}}^{1/2}$, and evaluate it using Cholesky decomposition whose computational cost scales as n^3 where $n = 3N$ is the size of the matrix. BD simulations with fluctuating hydrodynamic interactions routinely employ[56,67–69] a Chebyshev polynomial based method for the computation of the matrix square root, which scales as $n^2\ell$, where ℓ is related to the square root of the ratio of the maximum and minimum eigenvalues of the diffusion tensor. It was shown, to a good approximation[68], that $\ell \sim N^{1/4}$, resulting in an overall scaling of $n^{2.25}$ that is less expensive than the Cholesky method. In the absence of a detailed analysis of the spectral properties of the diffusion tensor for a system with fluctuating IV and HI, it is difficult to estimate *a priori* the computational savings resulting from opting for the Chebyshev method over Cholesky's. Cognizant of the relatively short chain lengths studied in the present work ($N_\text{b} \leq 10$), we have therefore chosen to use the latter for the evaluation of $\boldsymbol{\mathcal{D}}^{1/2}$, and note that it would be worthwhile to examine the improvement of the numerical performance of the current approach by using alternative methods to evaluate the matrix square root.

As described in detail by Hütter and Öttinger[46], it is computationally more efficient to solve the SDE obtained from the kinetic interpretation of Eq. (27), given by

$$\begin{aligned} d\boldsymbol{\mathcal{Q}}^* &= \boldsymbol{\mathcal{A}}^*(\boldsymbol{\mathcal{Q}}^*)dt^* + \frac{1}{2}\left[\boldsymbol{\mathcal{D}}\left(\boldsymbol{\mathcal{Q}}^* + d\boldsymbol{\mathcal{Q}}^*\right) \cdot \boldsymbol{\mathcal{D}}^{-1}\left(\boldsymbol{\mathcal{Q}}^*\right) + \boldsymbol{\mathcal{I}}\right] \cdot \boldsymbol{\mathcal{D}}^{1/2} \cdot\, d\boldsymbol{\mathcal{W}}^* \\ &= \boldsymbol{\mathcal{A}}^*(\boldsymbol{\mathcal{Q}}^*)dt^* + \boldsymbol{\mathcal{D}}^{1/2} \diamond d\boldsymbol{\mathcal{W}}^*, \end{aligned} \tag{34}$$

as compared to the numerical integration of the equivalent Itô interpretation given by Eq. (30). This manoeuvre replaces the calculation of the divergence of the diffusion tensor by that of its inverse. The quantity $\boldsymbol{\mathcal{I}}$ that appears in eq. (34) is a block matrix of size $N \times N$, whose each entry is the 3×3 identity matrix $\boldsymbol{\delta}$.

A predictor-corrector algorithm for the numerical integration of Eq. (34) is constructed next, following the steps detailed in Ref. 46. Equations (35)-(36) are in their dimensionless form, with the asterisk superscript omitted for notational simplicity.

Predictor step

$$\boldsymbol{\mathcal{Q}}^{(\text{p})}(t_{i+1}) = \boldsymbol{\mathcal{Q}}(t_i) + \boldsymbol{\mathcal{A}}\left(\boldsymbol{\mathcal{Q}}(t_i)\right) dt + \boldsymbol{\mathcal{D}}^{1/2}\left(\boldsymbol{\mathcal{Q}}(t_i)\right) \cdot \Delta\boldsymbol{\mathcal{W}} \tag{35}$$

Corrector step

$$\begin{aligned} \boldsymbol{\mathcal{Q}}(t_{i+1}) = \boldsymbol{\mathcal{Q}}(t_i) &+ \frac{1}{2}\left\{\boldsymbol{\mathcal{A}}\left(\boldsymbol{\mathcal{Q}}^{(\text{p})}(t_{i+1})\right) + \boldsymbol{\mathcal{A}}\left(\boldsymbol{\mathcal{Q}}(t_i)\right)\right\} dt \\ &+ \frac{1}{2}\left\{\boldsymbol{\mathcal{D}}\left(\boldsymbol{\mathcal{Q}}^{(\text{p})}(t_{i+1})\right) \cdot \boldsymbol{\mathcal{D}}^{-1}\left(\boldsymbol{\mathcal{Q}}(t_i)\right) + \boldsymbol{\mathcal{I}}\right\} \cdot \boldsymbol{\mathcal{D}}^{1/2}\left(\boldsymbol{\mathcal{Q}}(t_i)\right) \cdot \Delta\boldsymbol{\mathcal{W}} \end{aligned} \tag{36}$$

Hütter and Öttinger[46] note that the two-step numerical integration scheme mentioned above is weakly convergent to first order in the time-step width Δt.

Eq. 32 ensures that the governing stochastic differential equation, given by eq. (34), satisfies the fluctuation-dissipation theorem. We further illustrate this point in Sec. SV of the Supplementary Material, by verifying that the probability distribution of the lengths of the end-to-end vector of a ten-bead chain with IV and HI at equilibrium, obtained by numerically integrating eq. (34) in the absence of flow, agrees with the analytical expression.

A thermodynamically consistent stress tensor expression for chains with fluctuating internal friction and hydrodynamic interactions may be derived using the Kramers-Kirkwood relation[13], as suggested by Hua and Schieber[70]. We therefore have

$$\boldsymbol{\tau}_{\mathrm{p}} = -n_{\mathrm{p}} \sum_{\nu=1}^{N_{\mathrm{b}}} \left\langle \boldsymbol{R}_{\nu} \boldsymbol{F}_{\nu}^{(h)} \right\rangle \tag{37}$$

where $\boldsymbol{R}_{\nu} = \boldsymbol{r}_{\nu} - \boldsymbol{r}_{\mathrm{c}}$ is the position of the ν^{th} bead with respect to the centre of mass of the chain, and $\boldsymbol{F}_{\nu}^{(h)}$ is the hydrodynamic drag force on the ν^{th} bead. Equation (37) may be recast, after some algebra, in terms of the connector vectors,

$$\boldsymbol{\tau}_{\mathrm{p}} = -n_{\mathrm{p}} \sum_{k=1}^{N_{\mathrm{b}}-1} \left\langle \boldsymbol{Q}_k \left[k_B T \frac{\partial \ln \Psi}{\partial \boldsymbol{Q}_k} + \boldsymbol{F}_k^{(\mathrm{c})} + K \left(\frac{\boldsymbol{Q}_k \boldsymbol{Q}_k}{Q_k^2} \right) \cdot [\![\dot{\boldsymbol{Q}}_k]\!] \right] \right\rangle \tag{38}$$

where the $N_{\mathrm{b}} \times (N_{\mathrm{b}} - 1)$ matrix, $B_{\nu k}$, is defined as $B_{\nu k} = (k/N) - \Theta(k - \nu)$ with $\Theta(k - \nu)$ denoting a Heaviside step function. Substituting the expression for $[\![\dot{\boldsymbol{Q}}_k]\!]$ from Eq. (23) into the above equation and simplifying (as described in Sec. SVII of the Supplementary Material), the dimensionless stress tensor expression is obtained as follows

$$\begin{aligned}
\frac{\boldsymbol{\tau}_{\mathrm{p}}}{n_{\mathrm{p}} k_B T} &= (N_{\mathrm{b}} - 1)\, \boldsymbol{\delta} - \left\langle \sum_{k=1}^{N_{\mathrm{b}}-1} \boldsymbol{Q}_k^* \boldsymbol{F}_k^{*(\mathrm{c})} \right\rangle - 2\epsilon \left\langle \sum_{k,j=1}^{N_{\mathrm{b}}-1} \left(\boldsymbol{M}_{kj} \cdot \boldsymbol{\kappa}^* \right)^T : \left[\frac{\boldsymbol{Q}_k^* \boldsymbol{Q}_j^* \boldsymbol{Q}_k^* \boldsymbol{Q}_k^*}{Q_k^{*2}} \right] \right\rangle \\
&+ \epsilon \left\langle \sum_{k,j=1}^{N_{\mathrm{b}}-1} \left[\boldsymbol{D}_{kj}^T : \boldsymbol{Q}_k^* \boldsymbol{F}_j^{*(\mathrm{s})} \right] \frac{\boldsymbol{Q}_k^* \boldsymbol{Q}_k^*}{Q_k^{*2}} \right\rangle - \epsilon \left\langle \sum_{k,j=1}^{N_{\mathrm{b}}-1} \left(\frac{\boldsymbol{Q}_k^* \boldsymbol{Q}_k^*}{Q_k^{*2}} \right) \boldsymbol{Q}_k^* \cdot \underline{\left[\frac{\partial}{\partial \boldsymbol{Q}_j^*} \cdot \boldsymbol{D}_{kj}^T \right]} \right\rangle \\
&- \epsilon \left[\left\langle \sum_{k=1}^{N_{\mathrm{b}}-1} \left[\mathrm{tr}(\boldsymbol{D}_{kk}) - 2 \boldsymbol{D}_{kk} : \frac{\boldsymbol{Q}_k^* \boldsymbol{Q}_k^*}{Q_k^{*2}} \right] \frac{\boldsymbol{Q}_k^* \boldsymbol{Q}_k^*}{Q_k^{*2}} \right\rangle + \left\langle \sum_{k=1}^{N_{\mathrm{b}}-1} \frac{\boldsymbol{Q}_k^* \boldsymbol{Q}_k^*}{Q_k^{*2}} \cdot \boldsymbol{D}_{kk} \right\rangle + \left\langle \sum_{k=1}^{N_{\mathrm{b}}-1} \boldsymbol{D}_{kk} \cdot \frac{\boldsymbol{Q}_k^* \boldsymbol{Q}_k^*}{Q_k^{*2}} \right\rangle \right]
\end{aligned} \tag{39}$$

The underlined term in Eq. (38), when summed over the j index, represents the divergence of the diffusion tensor, and is evaluated at each instance when the viscometric functions need to be computed. The method of random finite difference discussed in Refs. 54 & 55 is adopted for the calculation of this term. We provide a brief recap of this procedure below, wherein the divergence of a matrix may be evaluated as an ensemble average.

Considering an arbitrary configuration-dependent tensor $\boldsymbol{\mathcal{S}}(\boldsymbol{\mathcal{Q}})$ of size $\mathcal{N} \times \mathcal{N}$, and two independent Gaussian random vectors $\boldsymbol{\rho}_A$ and $\boldsymbol{\rho}_B$ such that $\langle \boldsymbol{\rho}_A \boldsymbol{\rho}_B \rangle_{\mathrm{RFD}} = \boldsymbol{I}$ where $\boldsymbol{I}$ is an identity matrix of the same size as $\boldsymbol{\mathcal{S}}$, and $\langle \dots \rangle_{\mathrm{RFD}}$ denotes an ensemble-average, where the subscript is used to highlight that the ensemble-size for the RFD procedure may be chosen independently of the number of polymer chain trajectories used for the calculation of observables. We may thus write

$$\lim_{\delta \to 0} \frac{1}{\delta} \left\langle \left\{ \boldsymbol{\mathcal{S}} \left(\boldsymbol{\mathcal{Q}} + \frac{\delta}{2} \boldsymbol{\rho}_A \right) - \boldsymbol{\mathcal{S}} \left(\boldsymbol{\mathcal{Q}} - \frac{\delta}{2} \boldsymbol{\rho}_A \right) \right\} \boldsymbol{\rho}_B \right\rangle_{\mathrm{RFD}} = \lim_{\delta \to 0} \frac{1}{\delta} \left\langle \frac{\partial \boldsymbol{\mathcal{S}}}{\partial \boldsymbol{\mathcal{Q}}} \right\rangle : \langle \boldsymbol{\rho}_A \boldsymbol{\rho}_B \rangle_{\mathrm{RFD}} = \frac{\partial}{\partial \boldsymbol{\mathcal{Q}}} \cdot \boldsymbol{\mathcal{S}} \tag{40}$$

A value of $\delta = 10^{-5}$ is chosen after testing for convergence. Similarly, an ensemble size of 5×10^3 for the RFD calculation is found to suffice for obtaining convergent results, and is subsequently employed for all the simulation runs.

The dynamics of polymer chain models with fluctuating internal friction and hydrodynamic interactions may be computed by numerically integrating eq. (34), where the use of the kinetic interpretation circumvents the calculation of the divergence of the diffusion tensor. In a prior work[36], a recursion-based approach was used to decouple the equations of motion for a freely draining coarse-grained model with internal friction in order to

obtain the governing Fokker-Planck equation for the system. The equivalent stochastic differential equation is obtained using an Itô interpretation, and its numerical integration requires the calculation of the divergence, $\sum_{k=1}^{N} (\partial/\partial \boldsymbol{Q}_k^*) \cdot \boldsymbol{V}_{jk}^T$, at each timestep. The formal definition of $\boldsymbol{V}_{jk}^T$ is based on a recurrence relation that is quite involved, and is provided in ref. 36. A consequence of the decoupling methodology is that a closed form (but recursive) relationship for the dependence of $\boldsymbol{V}_{jk}$ on the connector vectors is obtained, which permitted the calculation of the divergence via a simple finite difference scheme. In the present work, however, there exists no closed form relationship for the diffusion tensor as a function of the chain configuration, and each evaluation of the block diffusion tensor would involve a matrix inversion (cf. eq. (21)), thus motivating the use of a divergence-free solution methodology. The algorithm used in the present work is an order of magnitude faster than that based on the decoupling method for the numerical solution of the governing stochastic differential equations, as illustrated in Sec. SIV of the Supplementary Material.

The stress tensor expression for polymer models with internal friction (with or without hydrodynamic interactions), however, contains a divergence term whose calculation cannot be avoided by a different choice of interpretation of the governing Fokker-Planck equation. In the decoupling approach, the matrix whose divergence is computed for the solution of the governing stochastic differential equation ($\boldsymbol{V}_{jk}$) is different from that whose divergence is evaluated in the stress tensor calculation ($\boldsymbol{\mu}_{kl}$). The two quantities are related to each other by

$$\boldsymbol{V}_{jl} = \sum_{j=1}^{N} \boldsymbol{A}_{jk} \cdot \boldsymbol{\mu}_{kl}, \tag{41}$$

where $\boldsymbol{A}_{jk}$ is the Rouse matrix defined in eq. (5)). In the methodology used in the present work, however, the divergence of the same quantity appears in both the governing stochastic differential equation and the stress tensor expression. This divergence needs to be evaluated only at the sampling instances where the viscosity needs to be computed, and not at each timestep. Therefore, if the interest is to only simulate the dynamics of the polymer chain, recording the changes in its configuration as a function of time, then the kinetic interpretation offers a manifestly faster computational route over the conventional Itô interpretation. For the calculation of the viscometric functions, the computational cost of using the methodology outlined in the present work would therefore scale with the number of sampling instances, unlike the recursion-based decoupling methodology. We reiterate that the one-to-all coupling between the connector vector velocities resulting from the inclusion of hydrodynamic interactions (cf. eq. (23)) implies that the applicability of the decoupling methodology is restricted to the free-draining case.

The bead-spring-dashpot chain is subjected to steady simple shear flow. The flow tensor, $\boldsymbol{\kappa}$ has the following

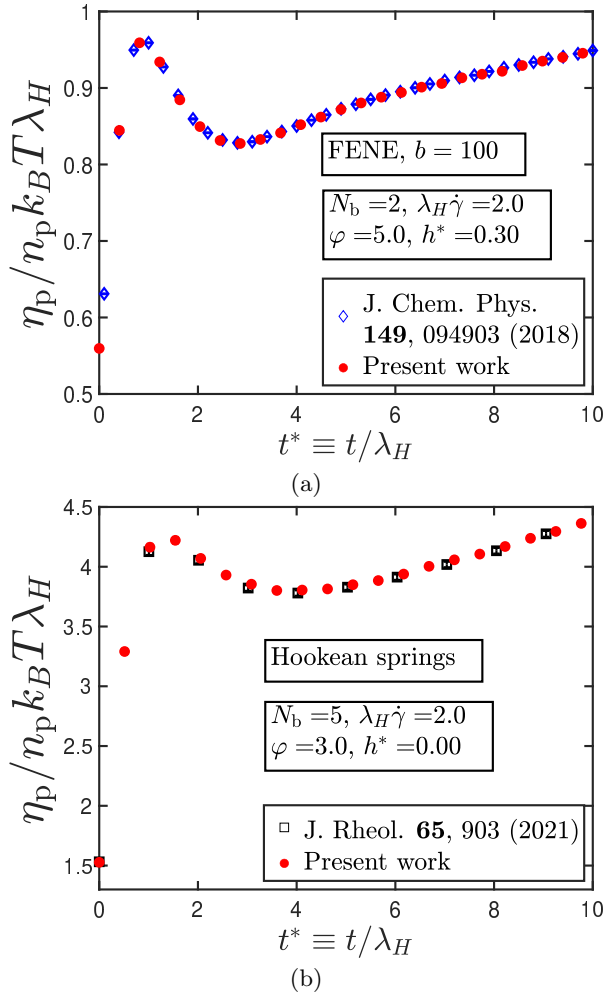

FIG. 2. (Color online) Comparison of shear viscosity predicted by present work against those calculated for (a) FENE dumbbells with internal viscosity and hydrodynamic interactions in Ref. 35, and (b) freely-draining Rouse chains with internal viscosity in Ref. 36. Error bars, which represent standard error of the mean, are roughly of the same size or smaller than the symbols used.

form

$$\boldsymbol{\kappa} \equiv \boldsymbol{\kappa}^* \, \lambda_H^{-1} = \dot{\gamma} \begin{pmatrix} 0 & 1 & 0 \\ 0 & 0 & 0 \\ 0 & 0 & 0 \end{pmatrix} \tag{42}$$

and the shear viscosity is defined as

$$\eta_p = -\frac{\tau_{p,xy}}{\dot{\gamma}} \tag{43}$$

where $\tau_{p,xy}$ refers to the xy element of the stress tensor.

The timestep used in the numerical integration procedure is dependent upon the shear rate and the magnitude of the internal friction parameter, with higher values of these parameters necessitating the use of smaller timesteps. For the highest value of the internal fric-

tion parameter considered in this work, $\varphi = 5.0$, values of $\Delta t^* = 10^{-3}$ for simulations of $\lambda_H\dot{\gamma} \leq 1.0$ and $\Delta t^* = 10^{-4}$ for $1.0 \leq \lambda_H\dot{\gamma} \leq 100.0$ have been found to result in convergent results [see Sec. SVI of the Supplementary Material]. Variance reduction[71] has been used in the evaluation of steady-shear viscometric functions at low shear rates ($\lambda_H\dot{\gamma} < 0.1$). Since internal friction and hydrodynamic interactions do not affect the configurational distribution function of polymer chains at equilibrium, the simulations are initiated by drawing the bead positions from the appropriate equilibrium distribution corresponding to Hookean or FENE springs. Internal friction or hydrodynamic interaction effects are turned on at $t^* = 0$, concomitantly as the shear flow is started. A rejection criterion[45] is employed that discards the instantaneous configuration if any spring is found to have exceeded its maximum permissible extension, $\sqrt{b}$. Each trajectory is run for a duration $t^*_{\max}$, until the shear viscosity attains a constant value, and the length of the trajectory depends upon the shear rate. For example, runs at $\lambda_H\dot{\gamma} = 10.0$ attain steady state by $t^*_{\max} = 60.0$, while the corresponding value at $\lambda_H\dot{\gamma} = 100.0$ is $t^*_{\max} = 30.0$. Simulations of Rouse chains, particularly with the inclusion of IV, are observed to require a longer time for the attainment of steady state, and hence we use $t^*_{\max} = 400.0$ for such chains at $\lambda_H\dot{\gamma} \geq 1.0$ and $t^*_{\max} = 200.0$ at $\lambda_H\dot{\gamma} < 1.0$. Averages are evaluated over an ensemble of $\mathcal{O}\left(10^4\right) - \mathcal{O}\left(10^5\right)$ individual trajectories.

Steady-shear viscosity profiles for the various models are scaled by their respective zero-shear rate value, $\eta^*_{\mathrm{p},0}$, calculated as the error-weighted mean of the viscosity values computed at the four lowest dimensionless shear rates, namely, $\lambda_H\dot{\gamma} = 0.001, 0.002, 0.005, 0.01$, after ensuring that shear-thinning has not set in at these shear rates. Shear rates are scaled by the relaxation time defined by $\lambda_{\mathrm{p}} = \eta_{\mathrm{p},0}/n_{\mathrm{p}}k_BT$.

III. RESULTS

A. Code Validation

The viscometric functions for FENE dumbbells with internal viscosity and hydrodynamic interactions subjected to simple shear flow have been evaluated in Ref. 35 by numerically integrating the governing stochastic differential equation obtained from an Itô interpretation of the Fokker-Planck equation using a semi-implicit predictor-corrector algorithm. For the special case of a dumbbell, the divergence of the diffusion tensor is known analytically. Material function predictions for free-draining Rouse chains with internal viscosity have been presented in Ref. 36, which also uses the Itô interpretation, a simple explicit Euler numerical integrator with the divergence of the diffusion tensor evaluated numerically, and the Giesekus expression for the stress tensor. We note that the Giesekus expression is not applicable for models with hydrodynamic interactions, and therefore cannot be used for the model considered in the present work.

In Fig. 2, the shear viscosity obtained using the methodology outlined in the present work are compared against data from Refs. 35 and 36. The excellent agreement between the results establishes the fidelity of the algorithm presented in this article.

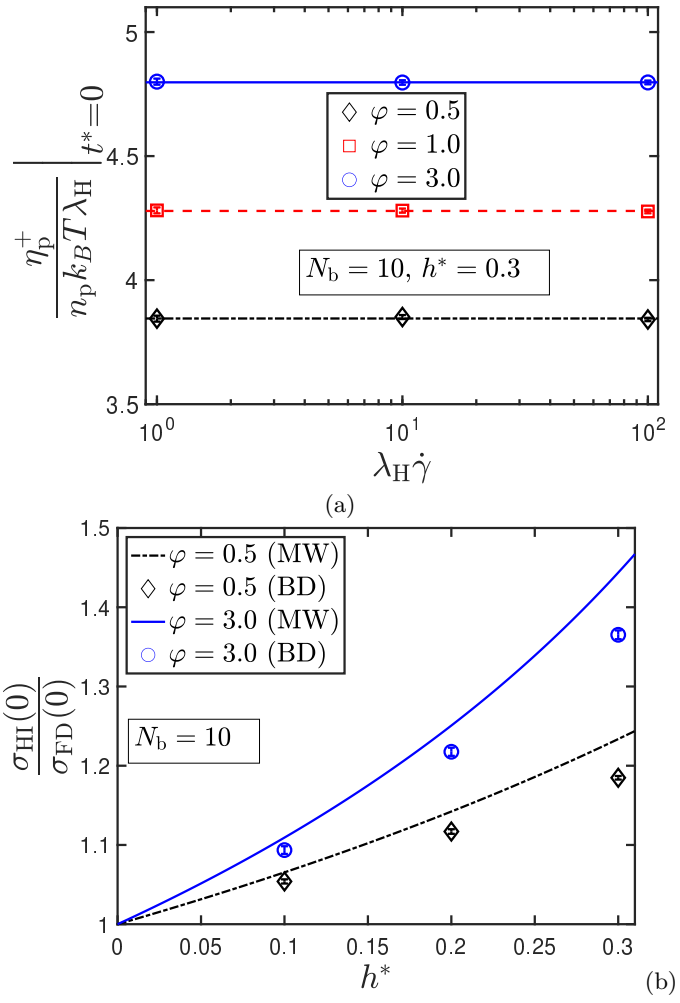

FIG. 3. (Color online) (a) Shear-rate independence of stress jumps observed in BD simulations of a ten-bead chain with Hookean springs and a hydrodynamic interaction parameter of $h^* = 0.3$, at various values of the internal friction parameter. The horizontal lines are error-weighted averages of the data points that they traverse. (b) Comparison of the stress jump ratio obtained from BD simulations (denoted by symbols) with the semi-analytical approximation of Manke and Williams[37] (indicated by lines). Error bars are roughly of the same size or smaller than the symbols used.

B. Stress jumps at the inception of steady shear flow

Having thus validated the numerical algorithm, this subsection presents results for the stress jump of bead-

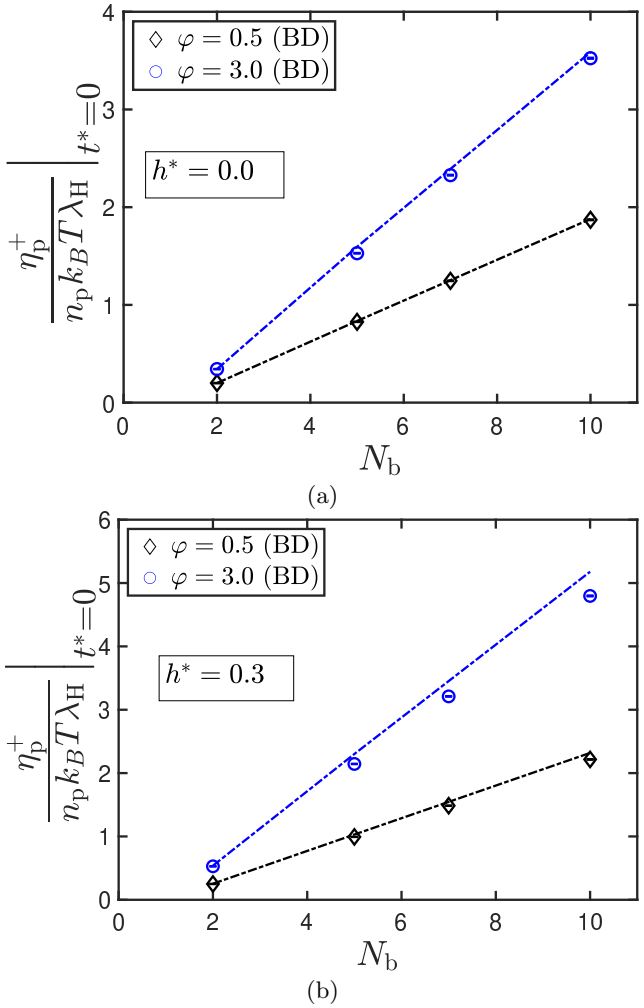

FIG. 4. (Color online) Comparison of stress jumps obtained from BD simulations (denoted by symbols) with the semi-analytical approximation of Manke and Williams[37] (indicated by lines) for Hookean bead-spring-dashpot chains of varying number of beads, (a) without and (b) with hydrodynamic interactions, for two different values of the internal friction parameter. Error bars are roughly of the same size or smaller than the symbols used.

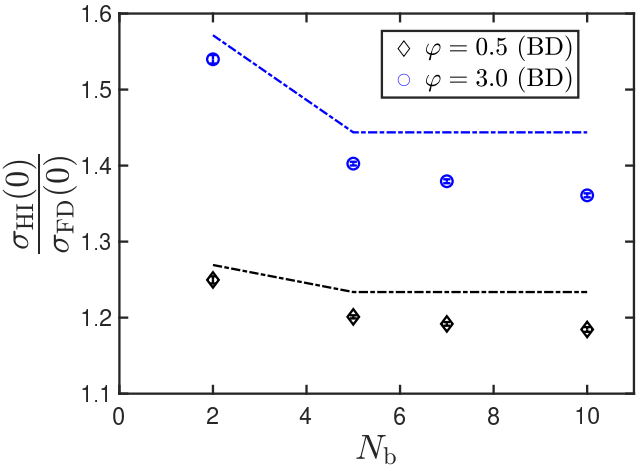

FIG. 5. (Color online) Stress jump ratio as a function of the chain length for Hookean bead-spring-dashpots. A value of $h^* = 0.3$ is used for simulations with hydrodynamic interactions. Predictions by Manke and Williams[37] are indicated by lines, while BD simulation results are denoted by symbols. Error bars are roughly of the same size or smaller than the symbols used.

spring-dashpot chains with Hookean springs. Polymer models with internal friction are known to exhibit a discontinuous jump in the viscosity at the inception of shear flow, and this is referred to as stress jump[24,35,36]. In Fig. 3 (a), the magnitudes of stress jump for a ten-bead chain with Hookean springs and three different values of the internal friction parameter, computed over a range of shear rates are plotted. The stress jump increases with the internal friction parameter, and is found to be independent of the shear rate, consistent with prior observations in the literature[37,72]. In the discussion and figures that follow in this section, the stress jump is computed at a dimensionless shear rate of $\lambda_H \dot{\gamma} = 10.0$.

Using a preaveraged form of hydrodynamic interaction tensor, Manke and Williams [37] derived a semi-analytical expression for the ratio of stress jumps for chains with and without hydrodynamic interactions. In figure 3 (b), the stress jump ratio evaluated over a range of h^* values are compared against the Manke and Williams [37] prediction, for two different values of the IV parameter. It is found that the semi-analytical predictions are close to the exact BD simulation results at small values of the internal friction and hydrodynamic interaction parameters, but overpredict the stress jump ratio at higher values of either φ or h^*. In order to probe the origin of this difference, the stress jump for chains with varying number of beads is computed and plotted in Fig. 4, for models with and without hydrodynamic interactions. A good agreement between the theoretical prediction and the numerically computed values is observed for the free-draining case across a range of N_b, at both low and high values of the internal friction parameter. The Manke and Williams [37] approximation is built on the assumption that the terminal connector vectors and the interior ones contribute equally to the stress jump of the chain. We have shown[36] previously, for free-draining chains, that this assumption becomes increasingly accurate as the number of beads in the model is increased, since the terminal connector vectors represent a smaller fraction of the overall length of the chain. With the inclusion of HI, however, the deviation of the semi-analytical approximation from the BD simulation result is seen to increase with the number of beads in the chain, and the departure is more easily perceived at higher values of the internal friction parameter, as illustrated in Fig. 4 (b). The shortcomings of the Manke and Williams [37] model is probably due to the 'pre-averaging' assumption, and the failure to account for

fluctuations in HI.

In Fig. 5, the stress jump ratio is plotted as a function of the number of beads in the chain. The stress jump values appear to approach a plateau as N_b is increased. The Manke and Williams [37] approximation is able to qualitatively predict this trend but differs in magnitude from the stress jump ratio obtained from exact BD simulations. The role of fluctuations in HI in determining the magnitude of the stress jump is evident from this figure.

C. Steady-shear viscometric functions

In this section, we analyze the steady shear viscosity of polymer models with various combinations of three non-linear effects: finite extensibility, internal friction, and hydrodynamic interactions in a ten-bead chain. The effect of IV and HI, considered separately, on the steady-shear viscosity of a chain with Hookean springs is highlighted in Figs. 6 (a) and (b). This figure will serve as the reference case for the rest of this section, as more combinations of the various nonlinear effects are considered. The simple Rouse model, with Hookean connecting springs between neighboring beads, predicts a constant value of the viscosity at all shear rates[13]. With the inclusion of hydrodynamic interactions, the viscosity undergoes mild shear-thinning, followed by thickening and culminating in a high shear-rate plateau. This behaviour, reported previously in Refs. 42,43,61, is also illustrated in Fig. 6 (a). Additionally, the zero-shear-rate viscosity of ten-bead Rouse chains with HI is lower than its free-draining counterpart.

The effect of internal friction on the material functions of free draining bead-spring-dashpot chains with Hookean springs has been examined in a previous work[36], and we restate the key features with respect to the shear viscosity variation here. As seen from Fig. 6 (b), the addition of IV effects to the Rouse model results in both a shear-thinning and thickening of the viscosity. An increase in the value of the IV parameter from $\varphi = 1.0$ to $\varphi = 5.0$ causes both the shear-thinning and thickening to increase. The critical shear rate at which the onset of shear-thickening is observed, however, remains largely unaffected by φ. Furthermore, the zero-shear rate viscosity for models with IV is also unaffected by φ, in agreement with previous theoretical and numerical predictions[36,59]. A comparison between Fig. 6 (a) and 6 (b) reveals that the magnitude of both shear-thinning and thickening induced by internal viscosity is larger than that due to hydrodynamic interactions, most noticeable for the $\varphi = 5.0$ case.

In Fig. 7, the shear viscosity of Rouse chains with fluctuating IV and hydrodynamic interactions is plotted as a function of shear rate, for two different values of the internal friction parameter. A comparison with Fig. 6 (b) reveals that the effect of inclusion of HI is least perceptible at low and moderate shear rates ($\lambda_p\dot{\gamma} \leq 15$), with the shear viscosity undergoing a mild-thinning following

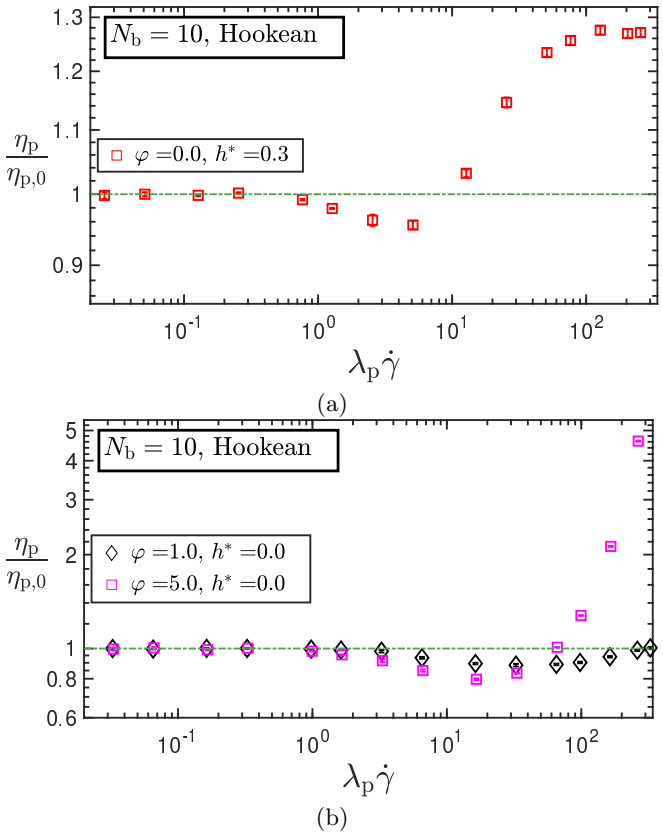

FIG. 6. (Color online) Scaled shear viscosity as a function of the dimensionless shear rate, for a ten-bead Rouse chain with (a) hydrodynamic interactions ($h^* = 0.3$) and (b) internal friction. Error bars are roughly of the same size or smaller than the symbols used.

the Newtonian plateau. The effect of HI, however, becomes more perceptible at higher shear rates. For freely-draining chains with $\varphi = 1$, the scaled viscosity does not rise above unity over the range of shear rates considered. The inclusion of hydrodynamic interactions, however, aids the shear-thickening effect, causing the viscosity for the $\varphi = 1$ to rise above unity at a smaller value of the shear rate. This cooperative interplay between internal viscosity and hydrodynamic interactions is less perceptible, however, at higher values of the IV parameter.

The inclusion of finite extensibility causes the viscosity to decrease as a function of the shear rate, with a power-law exponent of $-2/3$, as illustrated in Fig. 8 (a). This exponent is unaltered by the inclusion of HI, as seen from Fig. 8 (b). The interplay between finite extensibility and hydrodynamic interactions has been examined extensively in Refs. 61 & 43. At large enough values of the b parameter, implying a high degree of extensibility, coarse grained models exhibit a thinning-thickening-thinning pattern in the shear viscosity, with the onset of the high shear-rate thinning attributed to the finite extensibility of the connecting springs. The singular limit

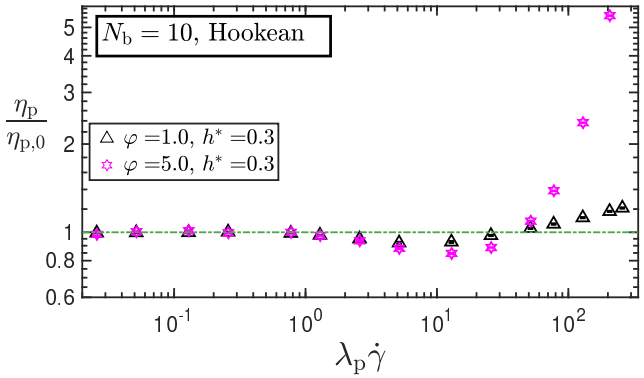

FIG. 7. (Color online) Shear viscosity of Rouse chains with fluctuating hydrodynamic interactions ($h^* = 0.3$), at two values of the internal friction parameter, $\varphi = 1.0$ and $\varphi = 5.0$. Error bars are roughly of the same size or smaller than the symbols used.

$b \to \infty$ represents the Hookean spring, and there is no second shear-thinning regime for this special case, as the viscosity reaches a high-shear rate plateau, as already seen in Fig. 6 (a). Below a threshold value of the b parameter (≈ 1000), however, the thickening at intermediate shear rates vanishes, and the shear viscosity thins continuously.

Aside from bead-spring-chain representations, a prominent choice for the modeling of dilute polymer solutions is bead-rod-chains, where the centres of friction are joined by rigid, inextensible rods. A crucial difference in the shear viscosity profile of these two models is that while bead-spring-chains (with finite extensibility) predict an indefinite shear-thinning at high shear rates[56,73], the bead-rod-chain predicts a second Newtonian plateau at high shear rates, following a shear-thinning regime[14,74–76]. This distinguishing feature remains true both in the presence and absence of fluctuating hydrodynamic interactions. Any discussion about the shear-thinning exponent in bead-rod-chain models, therefore, is applicable to the regime preceding the second Newtonian plateau. A detailed exposition on the shear-thinning phenomenon in dilute and semi-dilute polymer solutions, along with an extensive review of pertinent literature, is available in ref. 77.

While modeling a polymer chain of fixed length, increasing the number of rods corresponds to an increase in the flexibility of the model. In a simulation of freely-draining bead-rod chains[74], an increase in the number of rods from two to twenty results in an increase in the magnitude of the shear-thinning exponent, from (1/3) to (1/2). An exponent of $-(6/11)$ has been observed in BD simulations of bead-rod chains by Doyle *et al.*[75] and in bead-spring chains by Jendrejack *et al.*[9]. A common method to increase the stiffness of bead-spring chain models is the introduction of a bending potential that penalizes torsional angle rotation. Multiparticle collision dynamics simulations of semiflexible polymer

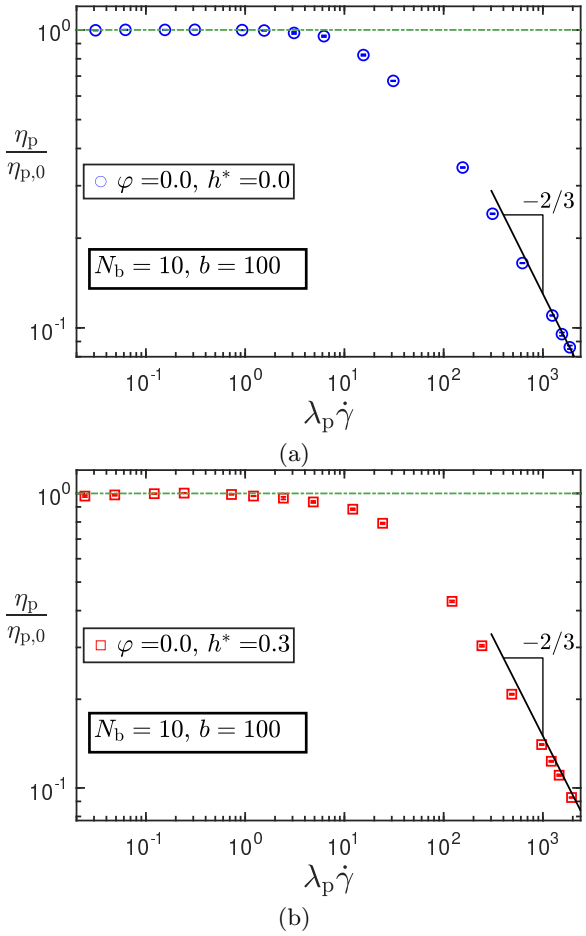

FIG. 8. (Color online) Shear viscosity of a dilute solution of ten-bead chains composed of finitely extensible springs, (a) without and (b) with hydrodynamic interactions. Error bars are roughly of the same size or smaller than the symbols used.

chains by Ryder and Yeomans[78] suggest that a shear-thinning exponent of $-(1/3)$ is reached as the strength of the bending potential is increased. These observations, therefore, serve to hint that the shear-thinning exponent is a measure of the static flexibility of the chain.

A comparison between Figs. 8 and 9 indicates that for the same level of discretization, the shear-thinning exponent changes from $-(2/3)$ to $-(1/3)$ upon the inclusion of a small value of the internal friction parameter ($\varphi = 1.0$). The qualitative pattern remains the same, with the shear-thinning appearing to continue indefinitely. It therefore seems that an inclusion of a small amount of IV decreases the static flexibility of the molecule, making it more stiff. At $\varphi = 1$, the steady-shear viscosity profile of a finitely extensible chain is not significantly affected by the presence of hydrodynamic interactions, as evident from Figs. 9 (a) and (b).

An increase in the IV parameter to a value of $\varphi = 5.0$ results in the appearance of a high-shear-rate plateau, following a shear-thinning-thickening pattern, as seen in figure 9 (c), a feature that is not observed in bead-spring-

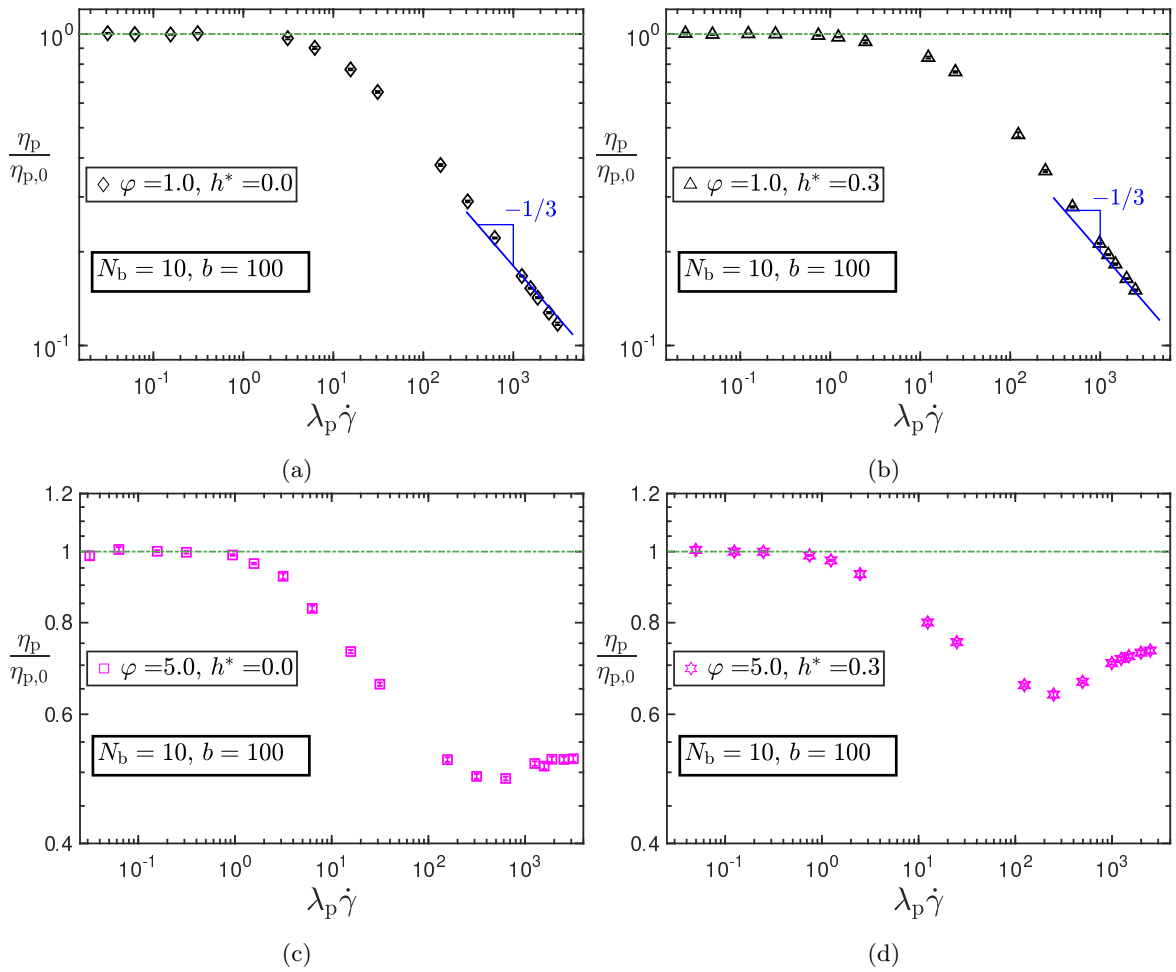

FIG. 9. (Color online) Shear viscosity of a ten-bead chain with FENE springs and (a) $\varphi = 1.0$, $h^* = 0.0$, (b) $\varphi = 5.0$, $h^* = 0.0$, (c) $\varphi = 1.0$, $h^* = 0.3$, and (d) $\varphi = 5.0$, $h^* = 0.3$. Error bars are roughly of the same size or smaller than the symbols used.

chain models without internal friction. A balance between the competing tendencies of the finite extensibility of the spring to decrease the viscosity at high shear rates, and that of IV to increase it could be a plausible explanation for this plateau. Experiments on dilute solutions of polystyrene in decalin[79](a θ-solvent) also show the appearance of a limiting viscosity at high-shear-rates, and has not been rationalized within the conventional coarse-grained framework that ignores short-time-scale viscous resistances to conformation.

The simultaneous inclusion of fluctuating internal viscosity and hydrodynamic interactions in a model with finitely extensible springs results in the onset of a thickening in the viscosity at high shear rates, as seen from figure 9 (d). This could be attributed to the cooperative shear-thickening effects of IV and HI dominating over the finite-extensibility-induced shear-thinning.

IV. CONCLUSIONS

A methodology for decoupling the connector vector velocities in coarse-grained polymer models with fluctuating internal friction and hydrodynamic interaction effects has been developed for the general case of a chain with N_b beads. This expands the scope for the treatment of flexible polymer models with IV and HI effects, for which solutions were previously available only for the $N_b = 2$ case[35,70]. The relevant stochastic differential equations are obtained by attaching a kinetic interpretation[46] to the governing Fokker-Planck equation, and integrated numerically using Brownian dynamics simulations. This method is validated by comparison against prior simulation results, where available, and is shown to be an order-of-magnitude faster than a previous, recursion-based technique[36] that is applicable only to free-draining models with internal friction. A thermodynamically consistent stress tensor expression for the model has been derived, and the divergence of the diffusion tensor appearing in this expression is evaluated

using a random finite difference approach[54,55].

While the semi-analytical approximation for the stress jump at the inception of shear flow in free-draining bead-spring-dashpot chains[24] compares excellently against exact numerical simulations[36], the corresponding approximation for such chains with pre-averaged hydrodynamic interactions[37] worsens with the number of beads in the chain, when compared against exact simulation results computed in this paper that account for fluctuations in both internal viscosity and hydrodynamic interactions.

The steady-shear viscosity of ten-bead chains with various combinations of finite extensibility, IV, and HI effects are presented over a range of shear rates. We find that while both IV and HI induce a shear-thinning followed by a thickening in the viscosity, the thickening effect due to the former is more pronounced than the latter. The inclusion of a small value of the internal friction parameter (in free-draining, finitely extensible chains) results in a shear-thinning exponent of $-(1/3)$, mimicking a rigid dumbbell, and this behavior is unaltered by the inclusion of hydrodynamic interactions. At higher values of the internal friction parameter, however, one observes a shear-thickening or a plateau in the viscosity at high shear rates, depending on whether HI is accounted for or not. The interplay between finite extensibility, IV, and HI effects, therefore, result in a variety of shear-viscosity profiles.

We recognize that the present work does not consider the effects of excluded volume interactions, which have been known to cause shear-thinning[14,15,56,80,81] in dilute polymer solutions. The inclusion of EV atop the various intramolecular interactions already considered in this work would certainly add more variety to what is already a rich tapestry of shear-thinning profiles. This additional dimension of the parameter space will be explored in a future publication. The key contributions of this work are: (a) the development of a solution algorithm that removes the one-to-all coupling between connector vector velocities in models with IV and HI, and (b) its efficient numerical integration using a kinetic interpretation. Given the continued interest from the biophysics community in understanding the roles of solvent-based and internal friction on the dynamics of proteins[5,82,83], the present work provides a mesoscopic simulation tool for answering such questions.

ACKNOWLEDGMENTS

R.K. thanks Prashant Patil, Aleksandar Donev, and Isaac Pincus for enlightening discussions. This work was supported by the MonARCH and MASSIVE computer clusters of Monash University, and the SpaceTime-2 computational facility of IIT Bombay. R. C. acknowledges SERB for funding (Project No. MTR/2020/000230 under MATRICS scheme). We also acknowledge the funding and general support received from the IITB-Monash Research Academy.

[1] A. Ansari, C. M. Jones, E. R. Henry, J. Hofrichter, and W. A. Eaton, Science **256**, 1796 (1992).
[2] S. J. Hagen, Curr. Protein Pept. Sci. **11**, 385 (2010).
[3] N. Samanta, J. Ghosh, and R. Chakrabarti, AIP Adv. **4**, 067102 (2014).
[4] N. Samanta and R. Chakrabarti, Physica A **450**, 165 (2016).
[5] D. Das, L. Arora, and S. Mukhopadhyay, J. Am. Chem. Soc. **144**, 1739 (2022).
[6] B. S. Khatri, M. Kawakami, K. Byrne, D. A. Smith, and T. C. B. McLeish, Biophys. J. **92**, 1825 (2007).
[7] Y. Murayama, H. Wada, and M. Sano, Eur. Phys. Lett. **79**, 58001 (2007).
[8] D. Vincenzi, Soft Matter **17**, 2421 (2021).
[9] R. M. Jendrejack, J. J. De Pablo, and M. D. Graham, J. Chem. Phys. **116**, 7752 (2002).
[10] R. G. Larson, J. Rheol. **49**, 1 (2005).
[11] C. M. Schroeder, E. S. G. Shaqfeh, and S. Chu, Macromolecules **37**, 9242 (2004).
[12] J. R. Prakash, Curr. Opin. Colloid Interface Sci. **43**, 63 (2019).
[13] R. B. Bird, C. F. Curtiss, R. C. Armstrong, and O. Hassager, *Dynamics of Polymeric Liquids - Volume 2 : Kinetic Theory* (John Wiley and Sons, New York, 1987).
[14] D. Petera and M. Muthukumar, J. Chem. Phys. **111**, 7614 (1999).
[15] J. R. Prakash, J. Rheol. **46**, 1353 (2002).
[16] P. Sunthar and J. R. Prakash, Macromolecules **38**, 617 (2005).
[17] P. Sunthar, D. A. Nguyen, R. Dubbelboer, J. R. Prakash, and T. Sridhar, Macromolecules **38**, 10200 (2005).
[18] A. Saadat and B. Khomami, J. Rheol. **59**, 1507 (2015).
[19] C. Sasmal, K.-W. Hsiao, C. M. Schroeder, and J. R. Prakash, J. Rheol. **61**, 169 (2017).
[20] M. E. Mackay, C. H. Liang, and P. J. Halley, Rheol. Acta **31**, 481 (1992).
[21] C.-H. Liang and M. E. Mackay, J. Rheol. **37**, 149 (1993).
[22] W. Kuhn and H. Kuhn, Helv. Chim. Acta **28**, 1533 (1945).
[23] A. Peterlin, J. Polym. Sci. A-2 Polym. Phys. **5**, 179 (1967).
[24] C. W. Manke and M. C. Williams, J. Rheol. **31**, 495 (1988).
[25] M. Fixman, J. Chem. Phys. **89**, 2442 (1988).
[26] M. Rubinstein and R. H. Colby, *Polymer Physics* (Oxford University Press, 2003).
[27] P.-G. de Gennes, *Scaling Concepts in Polymer Physics* (Cornell University Press, Ithaca, 1979).
[28] C. W. Manke and M. C. Williams, Macromolecules **18**, 2045 (1985).
[29] D. de Sancho, A. Sirur, and R. B. Best, Nat. Commun. **5**, 4307 (2014).
[30] I. Echeverria, D. E. Makarov, and G. A. Papoian, J. Am. Chem. Soc. **136**, 8708 (2014).
[31] H. C. Booij and P. H. van Wiechen, J. Chem. Phys. **52**, 5056 (1970).
[32] C. C. Hua and J. D. Schieber, J. Non-Newtonian Fluid Mech. **56**, 307 (1995).
[33] J. Ravi Prakash, "The kinetic theory of dilute solutions of flexible polymers: Hydrodynamic interaction," in *Advances in the Flow and Rheology of Non-Newtonian Fluids*, Rheology Series, Vol. 8, edited by D. Siginer, D. De Kee, and R. Chhabra (Elsevier, Netherlands, 1999) pp. 467–517, 1st ed.
[34] C. C. Hua, J. D. Schieber, and C. W. Manke, Rheol. Acta **35**, 225 (1996).
[35] R. Kailasham, R. Chakrabarti, and J. R. Prakash, J. Chem. Phys. **149**, 094903 (2018).
[36] R. Kailasham, R. Chakrabarti, and J. R. Prakash, J. Rheol. **65**, 903 (2021).
[37] C. W. Manke and M. C. Williams, J. Rheol. **36**, 1261 (1992).
[38] T. P. Dasbach, C. W. Manke, and M. C. Williams, J. Phys. Chem. **96**, 4118 (1992).
[39] R. Kailasham, R. Chakrabarti, and J. R. Prakash, Soft Matter **17**, 7133 (2021).
[40] B. S. Khatri and T. C. B. McLeish, Macromolecules **40**, 6770 (2007).
[41] W. Zylka and H. C. Öttinger, J. Chem. Phys. **90**, 474 (1989).

[42]W. Zylka, J. Chem. Phys. **94**, 4628 (1991).
[43]R. Prabhakar and J. R. Prakash, J. Rheol. **50**, 561 (2006).
[44]M. Fixman, Macromolecules **19**, 1195 (1986).
[45]H. C. Öttinger, *Stochastic Processes in Polymeric Fluids* (Springer, Berlin, 1996).
[46]M. Hütter and H. C. Öttinger, J. Chem. Soc; Faraday Trans. **94**, 1403 (1998).
[47]Y. L. Klimontovich, Physica A **163**, 515 (1990).
[48]Y. Klimontovich, Physica A **182**, 121 (1992).
[49]J. D. Schieber, Journal of Non-Newtonian Fluid Mechanics **45**, 47 (1992).
[50]C. D. Chau, G. J. Sevink, and J. G. Fraaije, J. Chem. Phys. **128**, 244110 (2008).
[51]M. De Corato, F. Greco, G. D'Avino, and P. L. Maffettone, J. Chem. Phys. **142**, 194901 (2015).
[52]M. De Corato, J. J. Slot, M. Hütter, G. D'Avino, P. L. Maffettone, and M. A. Hulsen, J. Comput. Phys. **316**, 632 (2016).
[53]P. S. Lang, B. Obermayer, and E. Frey, Phys. Rev. E **89**, 022606 (2014).
[54]B. Sprinkle, F. Balboa Usabiaga, N. A. Patankar, and A. Donev, J. Chem. Phys. **147**, 244103 (2017).
[55]B. Sprinkle, A. Donev, A. P. S. Bhalla, and N. Patankar, J. Chem. Phys. **150** (2019).
[56]R. Prabhakar and J. R. Prakash, J. Non-Newtonian Fluid Mech. **116**, 163 (2004).
[57]I. Pincus, A. Rodger, and J. R. Prakash, J. Non-Newtonian Fluid Mech. **285**, 104395 (2020).
[58]L. E. Wedgewood, Rheol. Acta **32**, 405 (1993).
[59]J. D. Schieber, J. Rheol. **37**, 1003 (1993).
[60]R. Sureshkumar and A. N. Beris, J. Rheol. **39**, 1361 (1995).
[61]A. J. Kishbaugh and A. J. McHugh, J. Non-Newtonian Fluid Mech. **34**, 181 (1990).
[62]J. Rotne and S. Prager, J. Chem. Phys. **50**, 4831 (1969).
[63]H. Yamakawa, *Modern Theory of Polymer Solutions* (Harper and Row, New York, 1971).
[64]W. Press, S. Teukolsky, W. Vetterling, and B. Flannery, *Numerical Recipes 3rd Edition: The Art of Scientific Computing* (Cambridge University Press, 2007).
[65]H. C. Öttinger, J. Non-Newtonian Fluid Mech. **26**, 207 (1987).
[66]L. E. Wedgewood and H. C. Öttinger, J. Non-Newtonian Fluid Mech. **27**, 245 (1988).
[67]M. Fixman, Macromolecules **19**, 1204 (1986).
[68]M. Kröger, A. Alba-Perez, M. Laso, and H. C. Ottinger, J. Chem. Phys. **113**, 4767 (2000).
[69]R. M. Jendrejack, M. D. Graham, and J. J. De Pablo, J. Chem. Phys. **113**, 2894 (2000).
[70]C. C. Hua and J. D. Schieber, Chem. Eng. Sci. **51**, 1473 (1996).
[71]N. J. Wagner and H. C. Öttinger, J. Rheol. **41**, 757 (1997).
[72]L. J. Gerhardt and C. W. Manke, J. Rheol. **38**, 1227 (1994).
[73]C.-C. Hsieh and R. G. Larson, J. Rheol. **48**, 995 (2004).
[74]T. W. Liu, J. Chem. Phys. **90**, 5826 (1989).
[75]P. S. Doyle, E. S. Shaqfeh, and A. P. Gast, J. Fluid Mech. **334**, 251 (1997).
[76]C. C. Hsieh, S. Jain, and R. G. Larson, J. Chem. Phys. **124**, 044911 (2006).
[77]S. Pan, D. A. Nguyen, B. Duenweg, P. Sunthar, T. Sridhar, and J. R. Prakash, J. Rheol. **62**, 845 (2018).
[78]J. F. Ryder and J. M. Yeomans, J. Chem. Phys. **125** (2006).
[79]I. Noda, Y. Yamada, and M. Nagasawa, J. Phys. Chem. **72**, 2890 (1968).
[80]A. V. Lyulin, D. B. Adolf, and G. R. Davies, Journal of Chemical Physics **111**, 758 (1999).
[81]S. Liu, B. Ashok, and M. Muthukumar, Polymer **45**, 1383 (2004).
[82]C. Xia, W. Kang, J. Wang, and W. Wang, J. Phys. Chem. B **125**, 2821 (2021).
[83]S. Mukherjee, S. Mondal, S. Acharya, and B. Bagchi, Phys. Rev. Lett. **128**, 108101 (2022).

Supplementary Material for: Shear viscosity for finitely extensible chains with fluctuating internal friction and hydrodynamic interactions

R. Kailasham,[1, a)] Rajarshi Chakrabarti,[2, b)] and J. Ravi Prakash[3, c)]

[1)] *Department of Chemical Engineering, Carnegie Mellon University, Pittsburgh, Pennsylvania - 15232, USA*

[2)] *Department of Chemistry, Indian Institute of Technology Bombay, Mumbai, Maharashtra - 400076, India*

[3)] *Department of Chemical Engineering, Monash University, Melbourne, VIC 3800, Australia*

(Dated: 25 April 2022)

arXiv:2204.10656v1 [cond-mat.soft] 22 Apr 2022

[a)]Electronic mail: rkailash@andrew.cmu.edu

[b)]Electronic mail: rajarshi@chem.iitb.ac.in

[c)]Electronic mail: ravi.jagadeeshan@monash.edu

SI. INTRODUCTION

The main paper derives the governing stochastic differential equations for coarse-grained polymer models with finite extensibility (FE), fluctuating internal friction (IV) and hydrodynamic interaction (HI) effects and outlines a methodology for their numerical integration, using Brownian dynamics (BD) simulations, based on a kinetic interpretation of the governing Fokker-Planck equation. A thermodynamically consistent stress expression is used to predict the steady shear viscosity as a function of the shear rate for models with various combinations of the three effects, namely, FE, IV, and HI. Additional details corresponding to various aspects of the study are presented here.

This document is organized as follows. Section SII establishes that the Fokker-Planck equation for a dumbbell with fluctuating IV and HI derived using the methodology developed in the present work, is identical to that obtained in Ref. 1. Sec. SIII illustrates empirically that the diffusion tensor for the present model is symmetric and positive definite. Sec. SIV establishes the equivalence between the present methodology and the decoupling algorithm developed in Ref. 2 for free-draining bead-spring-dashpot chains, and presents details on the computational cost and scaling for the two approaches. Sec. SV illustrates that the governing equations for the present model satisfy the fluctuation dissipation theorem, and Sec. SVI establishes that the BD simulation results presented in this work are time-step convergent. Lastly, Sec. SVII contains the derivation for the complete stress tensor expression used for the evaluation of shear viscosity from BD simulations. Summations are indicated explicitly, and the Einstein summation convention is not followed.

SII. COMPARISON AT DUMBBELL LEVEL

The dimensionless version of the Fokker-Planck equation for a bead-spring-dashpot chain with fluctuating hydrodynamic interactions has been presented as Eq. (27) in the main text, and is reproduced here

$$\frac{\partial \Psi^*}{\partial t^*} = -\sum_{j=1}^{N} \frac{\partial}{\partial \boldsymbol{Q}_j^*} \cdot \left\{ \left[\sum_{k=1}^{N} \boldsymbol{M}_{jk} \cdot (\boldsymbol{\kappa}^* \cdot \boldsymbol{Q}_k^*) - \frac{1}{4} \sum_{k=1}^{N} \boldsymbol{L}_{jk} \cdot \left(\frac{\partial \phi^*}{\partial \boldsymbol{Q}_k^*} \right) + \frac{1}{4} \sum_{k=1}^{N} \frac{\partial}{\partial \boldsymbol{Q}_k^*} \cdot \boldsymbol{L}_{jk}^T \right] \Psi^* \right\} \tag{S1}$$
$$+ \frac{1}{4} \sum_{j,k=1}^{N} \frac{\partial}{\partial \boldsymbol{Q}_j^*} \frac{\partial}{\partial \boldsymbol{Q}_k^*} : \left[\boldsymbol{L}_{jk}^T \Psi^* \right]$$

where we have introduced the notation $\boldsymbol{L}_{jk} = 2\boldsymbol{D}_{jk}$. For the case of a dumbbell, setting the number of springs, $N = 1$ in Eq. (S1) and denoting $\boldsymbol{Q}_1$ simply as $\boldsymbol{Q}$, we obtain

$$\frac{\partial \Psi^*}{\partial t^*} = -\frac{\partial}{\partial \boldsymbol{Q}^*} \cdot \left\{ \left[\boldsymbol{M}_{11} \cdot (\boldsymbol{\kappa}^* \cdot \boldsymbol{Q}^*) - \frac{1}{4} \boldsymbol{L}_{11} \cdot \left(\frac{\partial \phi^*}{\partial \boldsymbol{Q}^*} \right) + \frac{1}{4} \frac{\partial}{\partial \boldsymbol{Q}^*} \cdot \boldsymbol{L}_{11}^T \right] \Psi^* \right\} \tag{S2}$$
$$+ \frac{1}{4} \frac{\partial}{\partial \boldsymbol{Q}^*} \frac{\partial}{\partial \boldsymbol{Q}^*} : \left[\boldsymbol{L}_{11}^T \Psi^* \right]$$

From the development presented in the main text

$$\beta^* = \left[1 - \frac{\alpha}{Q^*} \left(\mathscr{A} + \mathscr{B} \right) \right] \tag{S3}$$

$$\alpha = \frac{3}{4} \sqrt{\pi} h^* \tag{S4}$$

$$\tilde{\boldsymbol{A}}_{11} = 2\left(\boldsymbol{\delta} - \zeta\Omega\right) \tag{S5}$$

$$\tilde{\boldsymbol{Z}}_{11} = 2\beta^* \left(\frac{\boldsymbol{Q}^*\boldsymbol{Q}^*}{\boldsymbol{Q}^{*2}}\right) \tag{S6}$$

$$\boldsymbol{Y}_{11} = \left[\boldsymbol{\delta} - \frac{\epsilon\beta^*}{\epsilon\beta^*+1}\frac{\boldsymbol{Q}^*\boldsymbol{Q}^*}{\boldsymbol{Q}^{*2}}\right] \tag{S7}$$

$$\boldsymbol{X}_{11} = 2\left[\boldsymbol{\delta} - \frac{\epsilon\beta^*}{\epsilon\beta^*+1}\frac{\boldsymbol{Q}^*\boldsymbol{Q}^*}{\boldsymbol{Q}^{*2}}\right]\cdot\left(\boldsymbol{\delta} - \zeta\Omega\right) \tag{S8}$$

$$\boldsymbol{J}_{11} = \boldsymbol{\delta} \tag{S9}$$

and consequently,

$$\begin{aligned}
\boldsymbol{J}_{11}^{-1} &= \boldsymbol{\delta} \\
\boldsymbol{M}_{11} &= \left[\boldsymbol{\delta} - \frac{\epsilon\beta^*}{\epsilon\beta^*+1}\frac{\boldsymbol{Q}^*\boldsymbol{Q}^*}{\boldsymbol{Q}^{*2}}\right] \\
\boldsymbol{L}_{11} &= 2\left[\boldsymbol{\delta} - \frac{\epsilon\beta^*}{\epsilon\beta^*+1}\frac{\boldsymbol{Q}^*\boldsymbol{Q}^*}{\boldsymbol{Q}^{*2}}\right]\cdot\left(\boldsymbol{\delta} - \zeta\Omega\right) \\
&= 2\left\{\boldsymbol{\delta}\left[1 - \frac{\mathscr{A}\alpha}{Q^*}\right] - \left(\frac{B\alpha}{Q^*}\right)\frac{\boldsymbol{Q}^*\boldsymbol{Q}^*}{\boldsymbol{Q}^{*2}} - \frac{\epsilon\beta^{*2}}{\epsilon\beta^*+1}\frac{\boldsymbol{Q}^*\boldsymbol{Q}^*}{\boldsymbol{Q}^{*2}}\right\} \\
&= \boldsymbol{L}_{11}^T
\end{aligned} \tag{S10}$$

Substituting Eq. (S10) in Eq. (S2) and simplifying,

$$\begin{aligned}
\frac{\partial\Psi^*}{\partial t^*} = -\frac{\partial}{\partial\boldsymbol{Q}^*}\cdot\Bigg\{\Bigg[\Bigg[\boldsymbol{\delta} - \frac{\epsilon\beta^*}{\epsilon\beta^*+1}\frac{\boldsymbol{Q}^*\boldsymbol{Q}^*}{\boldsymbol{Q}^{*2}}\Bigg]\cdot\left(\boldsymbol{\kappa}^*\cdot\boldsymbol{Q}^* - \frac{1}{2}\left(\boldsymbol{\delta} - \zeta\Omega\right)\cdot\left(\frac{\partial\phi^*}{\partial\boldsymbol{Q}^*}\right)\right) \\
+ \frac{1}{2}\underline{\frac{\partial}{\partial\boldsymbol{Q}^*}\cdot\Bigg[\left(\boldsymbol{\delta} - \frac{\epsilon\beta^*}{\epsilon\beta^*+1}\frac{\boldsymbol{Q}^*\boldsymbol{Q}^*}{\boldsymbol{Q}^{*2}}\right)\cdot\left(\boldsymbol{\delta} - \zeta\Omega\right)\Bigg]}\Bigg]\Psi^*\Bigg\} \\
+ \frac{1}{2}\frac{\partial}{\partial\boldsymbol{Q}^*}\frac{\partial}{\partial\boldsymbol{Q}^*} : \left[\left(\boldsymbol{\delta} - \frac{\epsilon\beta^*}{\epsilon\beta^*+1}\frac{\boldsymbol{Q}^*\boldsymbol{Q}^*}{\boldsymbol{Q}^{*2}}\right)\cdot\left(\boldsymbol{\delta} - \zeta\Omega\right)\Psi^*\right]
\end{aligned} \tag{S11}$$

which is identical to the Fokker-Planck equation derived in Ref. 1, where the underlined divergence term is evaluated to be of the form $g_2\left(\boldsymbol{Q}^*/Q^*\right)$, where the scalar g_2 is a function of $\{\alpha, \epsilon, \mathscr{A}, \mathscr{B}, Q^*\}$ and its complete expression is given in Eqs. (A14) - (A18) of Appendix A in Ref. 1. We have therefore established that upon setting $N = 1$, the general Fokker-Planck equation for bead-spring-chains with IV and HI derived in the present work reduces to the dumbbell expression available in the literature[1].

SIII. SYMMETRICITY AND POSITIVE DEFINITENESS OF THE DIFFUSION TENSOR

In Fig. S1, the smallest eigenvalue, and the difference between the diffusion matrix ($\boldsymbol{\mathcal{L}} = 2\boldsymbol{\mathcal{D}}$) and its transpose, are plotted for two different values of the internal friction and the

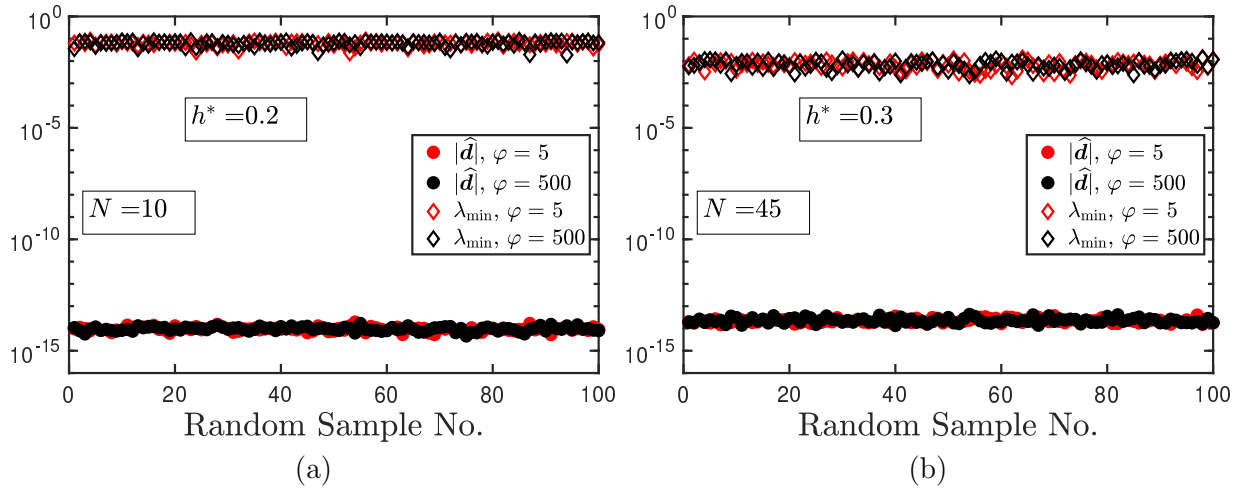

FIG. S1. Illustration of the positive definiteness and symmetricity of the diffusion tensor for a bead-spring chain of (a) ten and (b) forty-five springs, at different values of the internal friction and hydrodynamic interaction parameter.

hydrodynamic interaction parameter, for a hundred different random initial configurations. The smallest eigenvalues are positive, implying that the matrices are positive definite. The symmetricity of the matrix is quantified by calculating the difference as follows: firstly, the diffusion matrix and its transpose are subtracted, to generate a $3N \times 3N$ matrix. This matrix is reshaped to yield, $\widehat{\boldsymbol{d}}$, an array of $9N^2$ elements. The $2-$norm of this array is taken to be a numerical measure of the difference between the diffusion matrix and its transpose, as

$$||\boldsymbol{\mathcal{L}}^T - \boldsymbol{\mathcal{L}}|| \equiv |\widehat{\boldsymbol{d}}| = \sqrt{\left(\widehat{d}_1\right)^2 + \left(\widehat{d}_2\right)^2 + \cdots + \left(\widehat{d}_{9N^2}\right)^2} \tag{S12}$$

The difference computed in this manner is found to be $\mathcal{O}(10^{-14}) - \mathcal{O}(10^{-15})$ for both the values of chain length examined in Fig. S1, thereby establishing the symmetricity of the diffusion matrix in chains with fluctuating internal friction and hydrodynamic interactions.

SIV. COMPARISON AGAINST PRIOR WORK ON FREE-DRAINING BEAD-SPRING DASHPOT CHAINS

The present work provides an exact solution to the bead-spring-dashpot chain model with fluctuating IV and HI, which has thus far remained unsolved for the general case of $N > 1$. A comparison with prior art is therefore possible only in the free-draining limit, for which the solution was presented recently[2]. The dimensionless governing Fokker-Planck equation for free-draining bead-spring-dashpot chains derived in Ref. 2 may be recast as

$$\frac{\partial \Psi^*}{\partial t^*} = -\sum_{j=1}^{N} \frac{\partial}{\partial \boldsymbol{Q}_j^*} \cdot \left\{ \left[\sum_{k=1}^{N} \widehat{\boldsymbol{G}}_{jk} \cdot (\boldsymbol{\kappa}^* \cdot \boldsymbol{Q}_k^*) - \frac{1}{4} \sum_{k=1}^{N} \widehat{\boldsymbol{A}}_{jk} \cdot \left(\frac{\partial \phi^*}{\partial \boldsymbol{Q}_k^*} \right) + \frac{1}{4} \sum_{k=1}^{N} \frac{\partial}{\partial \boldsymbol{Q}_k^*} \cdot \widehat{\boldsymbol{A}}_{jk}^T \right] \Psi^* \right\} \tag{S13}$$

$$+ \frac{1}{4} \sum_{j,k=1}^{N} \frac{\partial}{\partial \boldsymbol{Q}_j^*} \frac{\partial}{\partial \boldsymbol{Q}_k^*} : \left[\widehat{\boldsymbol{A}}_{jk}^T \Psi^* \right]$$

where

$$\widehat{\boldsymbol{G}}_{jk} = \delta_{jk}\boldsymbol{\delta} - \left(\frac{\varphi}{2\varphi+1}\right)\boldsymbol{U}_{jk}$$
$$\widehat{\boldsymbol{A}}_{jk} = \boldsymbol{A}_{jk} - \left(\frac{\varphi}{2\varphi+1}\right)\boldsymbol{V}_{jk} \tag{S14}$$

with the definitions of the quantities ($\boldsymbol{U}_{jk}$ and $\boldsymbol{V}_{jk}$) obtained using the decoupling methodology appearing in the Supplementary Material to Ref. 2. We define the block matrices $\boldsymbol{\mathcal{G}}$ and $\boldsymbol{\mathcal{A}}$ whose elements are $\widehat{\boldsymbol{G}}_{jk}$ and $\widehat{\boldsymbol{A}}_{jk}$, respectively.

Equation (S13) is structurally identical to Eq. (S1), and the differences between the coefficient matrices are quantified by evaluating

$$||\boldsymbol{\mathcal{G}} - \boldsymbol{\mathcal{M}}|| = |\widehat{\boldsymbol{f}}| \tag{S15}$$

$$||\boldsymbol{\mathcal{A}} - \boldsymbol{\mathcal{L}}|| = |\widehat{\boldsymbol{e}}| \tag{S16}$$

as described in Eq. (S12). The differences computed in this manner are plotted in Fig. S2, for a thirty-spring chain at different values for the internal friction parameter. It is seen that both $|\widehat{\boldsymbol{f}}|$ and $|\widehat{\boldsymbol{e}}|$ increase with the internal friction parameter, and their magnitudes are nearly identical. The trend remains unaltered (not shown in plot) when a twenty-spring chain is considered.

From Eqs. (20) and (21) of the main text, it is clear that the construction of both $\boldsymbol{\mathcal{M}}$ and $\boldsymbol{\mathcal{L}}$ relies on the numerical computation of the inverse of $\boldsymbol{\mathcal{J}}$. In Fig. S3, the condition number of $\boldsymbol{\mathcal{J}}$ is plotted as a function of the internal friction parameter, for two different values of the number of springs in the chain. It is observed that the condition number scales quadratically with the IV parameter for $\varphi > 1$, and is practically insensitive to the chain length. We conclude, therefore, that the numerical error[3] associated with the inverse calculation of a matrix whose condition number scales with the IV parameter, is responsible for the perceived increase in the difference between the matrix coefficients calculated in the present work and those evaluated in Ref. 2 which does not rely on the numerical computation of matrix inverses.

In Fig. S4, the CPU time cost for the construction of the diffusion matrix, $\boldsymbol{\mathcal{L}}$, using the

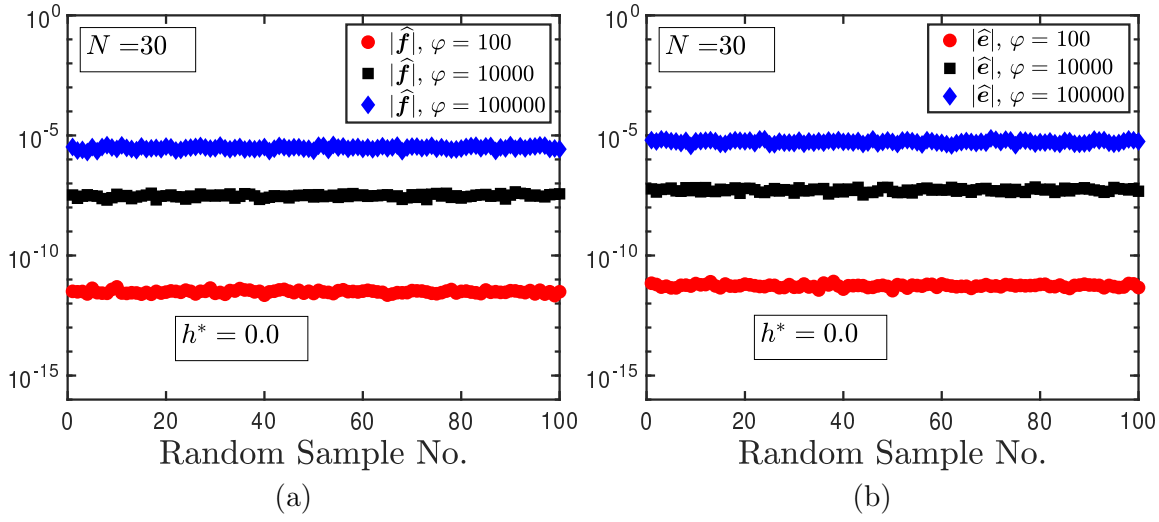

FIG. S2. Difference between the coefficient matrices computed by the methodology described in the present work and that calculated using the algorithm given in Ref. 2. Part (a) represents the difference denoted by Eq. (S15), and (b) corresponds to Eq. (S16)

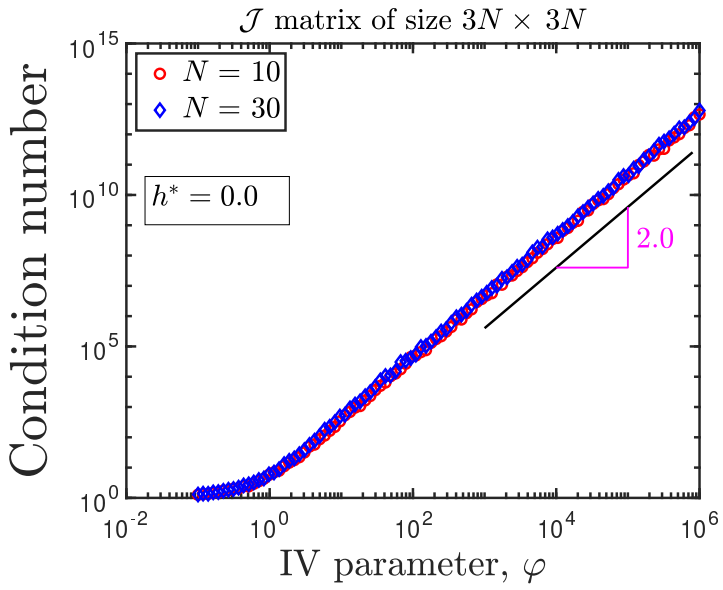

FIG. S3. Condition number of the $N \times N$ block matrix $\boldsymbol{\mathcal{J}}$, whose elements $\boldsymbol{J}_{jk}$ are the 3×3 matrices given by Eq. (18) of the main text, as a function of the internal friction parameter, φ, for two different values of the number of springs in the chain (N).

two approaches mentioned above is examined as a function of the internal friction parameter and the chain length. From Fig. S4 (a), it is observed that the execution time is practically unaffected by the IV parameter for two different values of the chain length considered. The time required by the algorithm developed in the present work, though, is about an order of magnitude smaller than that needed by the methodology developed in Ref. 2. In Fig. S4 (b), the scaling of the execution time is plotted as a function of the chain length for two values

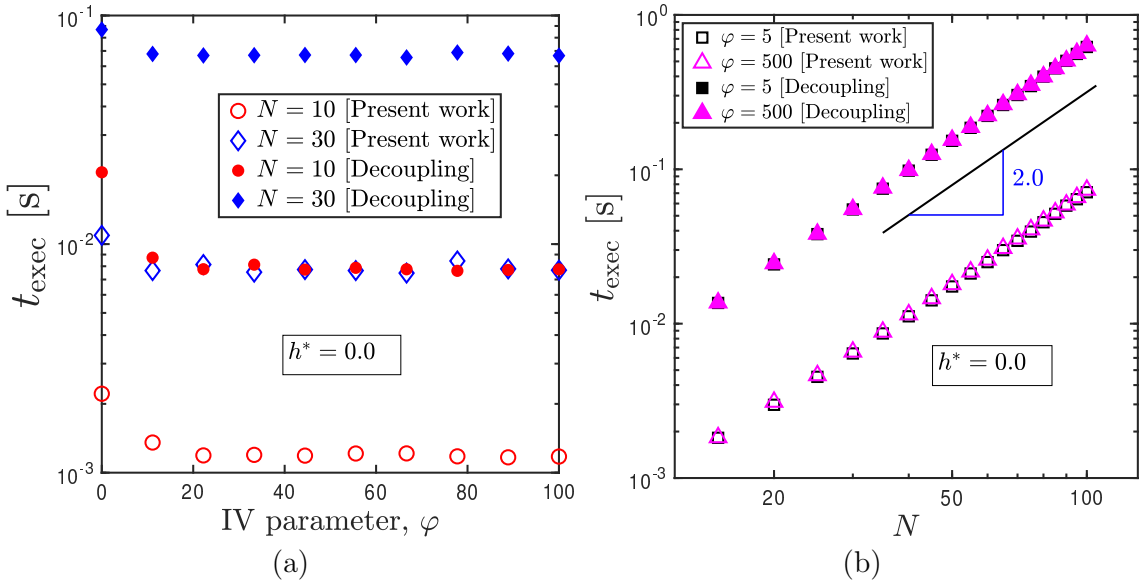

FIG. S4. A comparison of the time required for the construction of the diffusion matrix, $\boldsymbol{\mathcal{L}}$ using two approaches, plotted against (a) the internal friction parameter, and (b) the number of springs in the chain. The execution time reported corresponds to the average time needed for the construction of $\boldsymbol{\mathcal{L}}$, for a hundred different randomly chosen initial configurations of the chain.

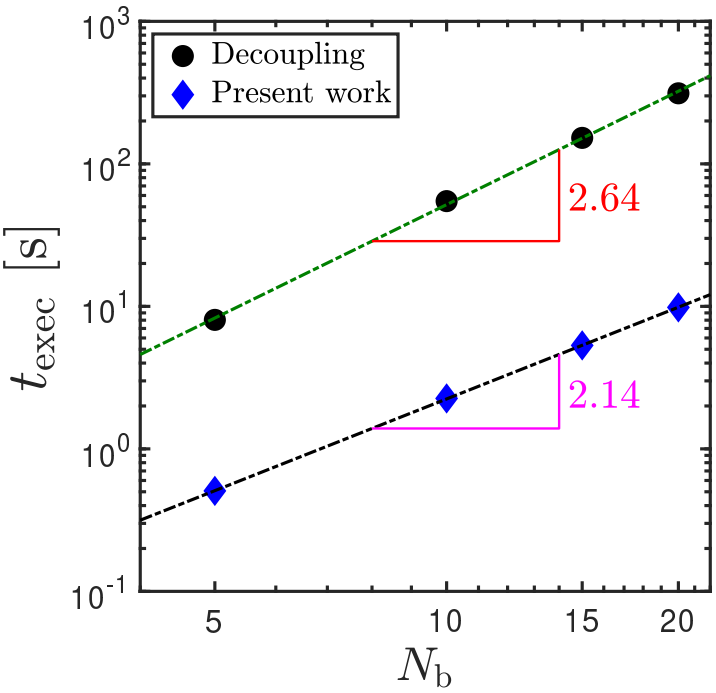

FIG. S5. A comparison of the execution time as a function of the number of beads, for equilibrium simulations of free-draining bead-spring-dashpot chains ($h^* = 0.0$) with an internal friction parameter of $\varphi = 5.0$.

of the internal friction parameter. While the computational cost for the two methods scale approximately as the square of the chain length, the method developed in the present work is about an order-of-magnitude faster than the decoupling-based approach used in Ref. 2.

A comparison of the computational cost of numerically integrating the governing stochastic differential equations for free-draining bead-spring-dashpots using the decoupling methodology[2], and the algorithm described in the present work is presented in Fig. S5. There is a $\sqrt{N}$ difference in the scaling of the execution time between the two methodologies, with $t_{\text{exec}} \sim N_{\text{b}}^{2.64}$ for the decoupling approach, and $t_{\text{exec}} \sim N_{\text{b}}^{2.14}$ for the present work. Additionally, the present method is an order-of-magnitude faster.

SV. SATISFACTION OF FLUCTUATION-DISSIPATION THEOREM

Internal friction and hydrodynamic interactions represent the dashpot- and solvent-mediated transfer of momentum between the beads in the chain, and do not feature in the Hamiltonian, $\mathcal{H}$, of the system, which contains contributions only from conservative intramolecular interactions. Consequently, it is expected that IV and HI do not affect the configurational distribution function of a chain at equilibrium, Ψ_{eq}, since $\Psi_{\text{eq}} \propto \exp[-\mathcal{H}/k_B T]$. The fluctuation-dissipation theorem (FDT) prescribes a relation between the fluctuations in the chain configuration and the various sources of friction (dissipation) experienced by the chain. The FDT is imposed in our model formulation by requiring that $\boldsymbol{\mathcal{B}} \cdot \boldsymbol{\mathcal{B}}^T = \boldsymbol{\mathcal{D}}$ in the governing stochastic differential equation (see eq. (32)) in the main text.

The probability distribution of the length of the vector running from bead μ to ν in a Rouse chain, $R^*_{\mu\nu} = |\boldsymbol{r}^*_\nu - \boldsymbol{r}^*_\mu|$, is known analytically[4], and may be written as follows

$$P^*\left(R^*_{\mu\nu}\right) = 4\pi\, R^{*2}_{\mu\nu} \left[\frac{1}{2\pi|\nu-\mu|}\right]^{3/2} \exp\left[-\frac{R^{*2}_{\mu\nu}}{2|\nu-\mu|}\right] \tag{S17}$$

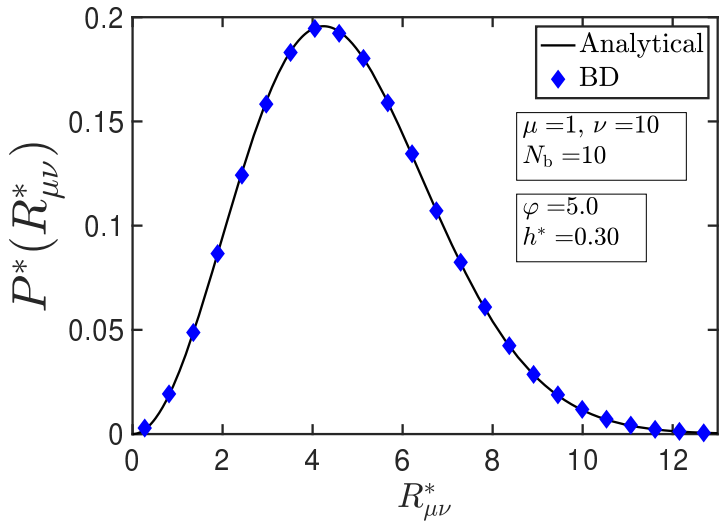

FIG. S6. Probability distribution of the lengths of the end-to-end vector of a ten-bead chain with internal friction and hydrodynamic interactions. Symbols are BD simulation results, and the line represents the analytical result given by eq. (S17).

In Fig. S6, the numerically computed probability distribution of the end-to-end vector of a ten-bead Rouse chain with internal friction and hydrodynamic interactions, evaluated by binning the output from $\mathcal{O}(5 \times 10^5)$ trajectories at the end of an equilibrium run of $t^*_{\max} = 10$ dimensionless times, is compared against the analytical result given by eq. (S17). The excellent agreement between the two results verifies that the fluctuation-dissipation theorem is indeed satisfied.

SVI. ESTABLISHING TIMESTEP CONVERGENCE

The calculation of shear viscosity at dimensionless shear rates $\lambda_H \dot{\gamma} < 0.1$ is performed using the variance reduction algorithm[5], while that for $\lambda_H \dot{\gamma} \geq 0.1$ does not use variance reduction. The choice of timestep (Δt^*) for integration is dictated by the value of the internal friction parameter, and the dimensionless shear rate.

In Fig. S7, the transient evolution of the shear viscosity at two different shear rates, computed using timestep widths that differ by a factor of ten, is plotted for the highest values of the internal friction and hydrodynamic interaction parameters considered in this work ($\varphi = 5.0, h^* = 0.3$). Given the agreement between the results at the different timesteps, we consider our numerical computations to be timestep convergent.

SVII. DERIVATION OF STRESS TENSOR EXPRESSION

The first step in the derivation of a usable stress tensor expression for the model under investigation is the conversion of the Kramers-Kirkwood expression,

$$\boldsymbol{\tau}_{\mathrm{p}} = -n_{\mathrm{p}} \sum_{\nu=1}^{N_{\mathrm{b}}} \left\langle \boldsymbol{R}_\nu \boldsymbol{F}_\nu^{(h)} \right\rangle , \tag{S18}$$

given in terms of the bead position vectors into its equivalent form using the connector vector notation. It is noted that $\boldsymbol{R}_\nu = \boldsymbol{r}_\nu - \boldsymbol{r}_{\mathrm{c}}$ is the position of the ν^{th} bead with respect to the centre of mass of the chain, and $\boldsymbol{F}_\nu^{(h)}$ is the hydrodynamic drag force on the ν^{th} bead. From

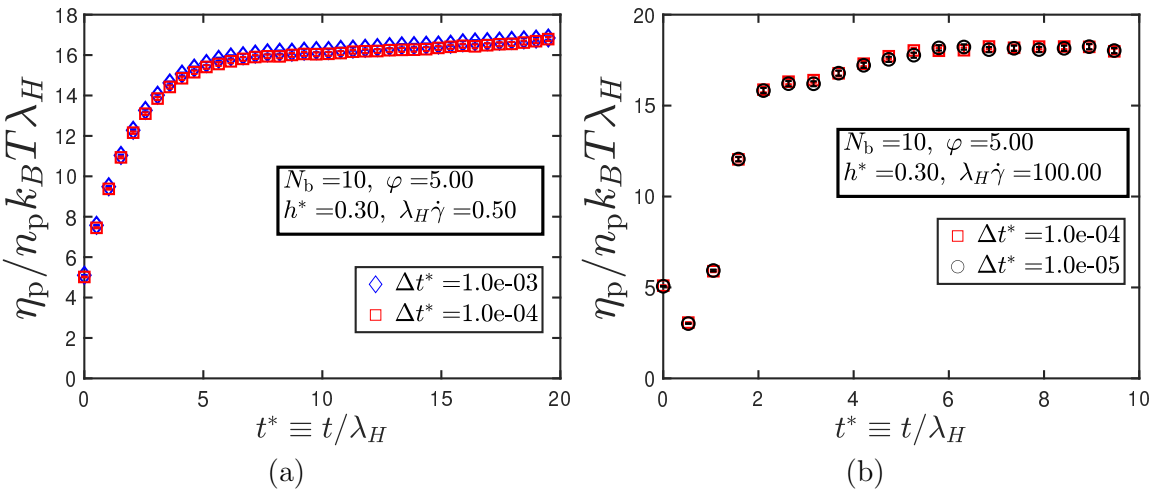

FIG. S7. Transient evolution of shear viscosity computed at two different timestep widths for a ten-bead chain with FENE springs of $b = 100$ and fluctuating internal friction and hydrodynamic interactions, at (a) dimensionless shear rates of $\lambda_H\dot{\gamma} = 0.5$, using variance reduction; and (b) $\lambda_H\dot{\gamma} = 100.0$.

Ref. 6, we have

$$\boldsymbol{F}_\nu^{(h)} = k_B T \frac{\partial \ln \psi}{\partial \boldsymbol{r}_v} - \boldsymbol{F}_\nu^{(\phi)} - \boldsymbol{F}_\nu^{(\mathrm{IV})} \tag{S19}$$

The configurational distribution function written in terms of the bead positions, $\psi(\boldsymbol{r}_1, \boldsymbol{r}_2, ..\boldsymbol{r}_{N_b})$ is equivalent to that written in terms of the internal coordinates $\Psi(\boldsymbol{Q}_1, \boldsymbol{Q}_2, ..., \boldsymbol{Q}_N)$ under conditions of homogeneous flow, where the distribution does not depend explicitly on the coordinates of the centre of mass. We may then write, using entry (F) of Table 15.4-1 in Bird *et al.*[4],

$$\frac{\partial \ln \psi}{\partial \boldsymbol{r}_v} = \sum_{k=1}^{N} \bar{B}_{k\nu} \frac{\partial \ln \Psi}{\partial \boldsymbol{Q}_k} \tag{S20}$$

with $\bar{B}_{k\nu} = \delta_{k+1,\nu} - \delta_{k\nu}$, $N = N_b - 1$. The total force on a bead consists of contributions from the springs and the excluded volume potential, i.e., $\boldsymbol{F}_\nu^{(\phi)} = \boldsymbol{F}_\nu^{(\mathrm{S})} + \boldsymbol{F}_\nu^{(\mathrm{EV})}$. We may then write

$$\boldsymbol{F}_\nu^{(\mathrm{S})} = -\sum_{k=1}^{N} \bar{B}_{k\nu} \boldsymbol{F}_k^{(\mathrm{c})} \tag{S21}$$

where

$$\boldsymbol{F}_k^{(\mathrm{c})} = H f(Q_k) \boldsymbol{Q}_k \tag{S22}$$

with

$$f(Q_k) = \begin{cases} 1 & \text{for Hookean springs,} \\ \dfrac{1}{1 - (Q_k/Q_0)^2} & \text{for FENE springs.} \end{cases} \tag{S23}$$

Similarly, we have

$$\boldsymbol{F}_\nu^{(\mathrm{IV})} = -\sum_{k=1}^{N} \bar{B}_{k\nu} \boldsymbol{F}_k^{(\mathrm{IV})} \tag{S24}$$

with

$$\boldsymbol{F}_k^{(\mathrm{IV})} = K \frac{\boldsymbol{Q}_k \boldsymbol{Q}_k}{\boldsymbol{Q}_k^2} \cdot [\![\dot{\boldsymbol{Q}}_k]\!] \tag{S25}$$

Using eqs. (S20), (S21), and (S24), $\boldsymbol{F}_\nu^{(h)}$ may be rewritten as

$$\boldsymbol{F}_\nu^{(h)} = \sum_{k=1}^{N} \bar{B}_{k\nu} \left[k_B T \frac{\partial \ln \Psi}{\partial \boldsymbol{Q}_k} + \boldsymbol{F}_k^{(\mathrm{c})} + \boldsymbol{F}_k^{(\mathrm{IV})} \right] \tag{S26}$$

From Eq. (11.6-4) in Bird *et al.*[4],

$$\boldsymbol{R}_\nu \equiv \boldsymbol{r}_\nu - \boldsymbol{r}_\mathrm{c} = \sum_{j=1}^{N} B_{\nu j} \boldsymbol{Q}_j \tag{S27}$$

with $B_{\nu j} = (j/N) - \Theta(j-\nu)$ with $\Theta(j-\nu)$ denoting a Heaviside step function. Thus we have

$$\boldsymbol{R}_\nu \boldsymbol{F}_\nu^{(h)} = \sum_{k=1}^{N} \sum_{j=1}^{N} B_{\nu j} \boldsymbol{Q}_j \bar{B}_{k\nu} \left[k_B T \frac{\partial \ln \Psi}{\partial \boldsymbol{Q}_k} + \boldsymbol{F}_k^{(\mathrm{c})} + \boldsymbol{F}_k^{(\mathrm{IV})} \right] \tag{S28}$$

and

$$\sum_{\nu=1}^{N_\mathrm{b}} \left\langle \boldsymbol{R}_\nu \boldsymbol{F}_\nu^{(h)} \right\rangle = \sum_{\nu=1}^{N_\mathrm{b}} \sum_{k=1}^{N} \sum_{j=1}^{N} \left(\bar{B}_{k\nu} B_{\nu j} \right) \boldsymbol{Q}_j \left[k_B T \frac{\partial \ln \Psi}{\partial \boldsymbol{Q}_k} + \boldsymbol{F}_k^{(\mathrm{c})} + \boldsymbol{F}_k^{(\mathrm{IV})} \right] \tag{S29}$$

Using

$$\sum_{\nu=1}^{N_\mathrm{b}} \bar{B}_{k\nu} B_{\nu j} = \delta_{kj} \tag{S30}$$

and combining eq. (S29) with eq. S18, the Kramers-Kirkwood expression is rewritten as

$$\boldsymbol{\tau}_\mathrm{p} = -n_\mathrm{p} \sum_{k=1}^{N_\mathrm{b}-1} \left\langle \boldsymbol{Q}_k \left[k_B T \, \frac{\partial \ln \Psi}{\partial \boldsymbol{Q}_k} + \boldsymbol{F}_k^{(\mathrm{c})} + \boldsymbol{F}_k^{(\mathrm{IV})} \right] \right\rangle \tag{S31}$$

which is equivalent to eq. (38) in the main text. The decoupled expression for $[\![\dot{\boldsymbol{Q}}_k]\!]$ has been derived in eq. (24) of the main text, and is reproduced below

$$[\![\dot{\boldsymbol{Q}}_k]\!] = \sum_{j=1}^{N} \boldsymbol{M}_{kj} \cdot (\boldsymbol{\kappa} \cdot \boldsymbol{Q}_j) - \frac{2 k_B T}{\zeta} \sum_{j=1}^{N} \boldsymbol{D}_{kj} \cdot \left(\frac{\partial \ln \Psi}{\partial \boldsymbol{Q}_j} \right) - \frac{2}{\zeta} \sum_{j=1}^{N} \boldsymbol{D}_{kj} \cdot \left(\frac{\partial \phi}{\partial \boldsymbol{Q}_j} \right) \tag{S32}$$

Combining eq. (S32) with eq. (S25) and simplifying, eq. (S29) becomes

$$\begin{aligned}
\sum_{\nu=1}^{N_\mathrm{b}} \left\langle \boldsymbol{R}_\nu \boldsymbol{F}_\nu^{(h)} \right\rangle &= k_B T \sum_{k=1}^{N} \left\langle \boldsymbol{Q}_k \frac{\partial \ln \Psi}{\partial \boldsymbol{Q}_k} \right\rangle + \sum_{k=1}^{N} \left\langle \boldsymbol{Q}_k \boldsymbol{F}_k^{(\mathrm{c})} \right\rangle \\
&+ K \sum_{k,j=1}^{N} \left\langle \left(\frac{\boldsymbol{Q}_k \boldsymbol{Q}_k \boldsymbol{Q}_k}{Q_k^2} \right) \cdot \boldsymbol{M}_{kj} \cdot (\boldsymbol{\kappa} \cdot \boldsymbol{Q}_j) \right\rangle - \frac{2 k_B T K}{\zeta} \sum_{k,j=1}^{N} \left\langle \left(\frac{\boldsymbol{Q}_k \boldsymbol{Q}_k \boldsymbol{Q}_k}{Q_k^2} \right) \cdot \boldsymbol{D}_{kj} \cdot \left(\frac{\partial \ln \Psi}{\partial \boldsymbol{Q}_j} \right) \right\rangle \\
&- \frac{2K}{\zeta} \sum_{k,j=1}^{N} \left\langle \left(\frac{\boldsymbol{Q}_k \boldsymbol{Q}_k \boldsymbol{Q}_k}{Q_k^2} \right) \cdot \boldsymbol{D}_{kj} \cdot \boldsymbol{F}_j^{(\mathrm{c})} \right\rangle
\end{aligned} \tag{S33}$$

The terms on the RHS of eq. (S33) are simplified as shown below. Firstly,

$$\left\langle \boldsymbol{Q}_k \frac{\partial \ln \Psi}{\partial \boldsymbol{Q}_k} \right\rangle = \left[\sum_{\mu,\omega} \int \left(\frac{\partial \Psi}{\partial Q_k^\mu} \right) Q_k^\omega \, d\boldsymbol{\mathcal{Q}} \right] \boldsymbol{e}_\mu \boldsymbol{e}_\omega \tag{S34}$$

where $d\boldsymbol{\mathcal{Q}} \equiv d\boldsymbol{Q}_1 d\boldsymbol{Q}_2 \cdots d\boldsymbol{Q}_N$ and $\boldsymbol{e}_\mu$ and $\boldsymbol{e}_\omega$ denote the unit vectors in Cartesian coordinates. Then,

$$\int \left(\frac{\partial \psi}{\partial Q_k^\mu} \right) Q_k^\omega \, d\boldsymbol{\mathcal{Q}} = \int \left[\frac{\partial}{\partial Q_k^\mu} \left(Q_k^\omega \Psi \right) - \psi \frac{\partial Q_k^\omega}{\partial Q_k^\mu} \right] d\boldsymbol{\mathcal{Q}} = \underline{\int \frac{\partial}{\partial Q_k^\mu} \left(Q_k^\omega \Psi \right) d\boldsymbol{\mathcal{Q}}} - \delta^{\mu\omega} \int \Psi \, d\boldsymbol{\mathcal{Q}} \tag{S35}$$

The underlined term in Eq. (S35) vanishes due to the Gauss divergence theorem, and the integral in the second term is unity due to the normalization condition, and we thus have

$$\left\langle \boldsymbol{Q}_k \frac{\partial \ln \Psi}{\partial \boldsymbol{Q}_k} \right\rangle = -\boldsymbol{\delta} \tag{S36}$$

We may similarly write

$$\left\langle \left(\frac{\boldsymbol{Q}_k \boldsymbol{Q}_k \boldsymbol{Q}_k}{Q_k^2} \right) \cdot \boldsymbol{D}_{kj} \cdot \left(\frac{\partial \ln \Psi}{\partial \boldsymbol{Q}_j} \right) \right\rangle = \left[\sum_{\mu,\omega} \sum_{m,n} \int \frac{Q_k^\mu Q_k^\omega Q_k^m}{Q_k^2} D_{kj}^{mn} \frac{\partial \Psi}{\partial Q_j^n} d\boldsymbol{\mathcal{Q}} \right] \boldsymbol{e}_\mu \boldsymbol{e}_\omega \tag{S37}$$

and

$$\begin{aligned} \frac{Q_k^\mu Q_k^\omega Q_k^m}{Q_k^2} D_{kj}^{mn} \frac{\partial \Psi}{\partial Q_j^n} = \frac{\partial}{\partial Q_j^n} \left[\left(\frac{Q_k^\mu Q_k^\omega Q_k^m}{Q_k^2} \right) D_{kj}^{mn} \Psi \right] - \Psi D_{kj}^{mn} \frac{\partial}{\partial Q_j^n} \left[\frac{Q_k^\mu Q_k^\omega Q_k^m}{Q_k^2} \right] \\ - \Psi \left(\frac{Q_k^\mu Q_k^\omega Q_k^m}{Q_k^2} \right) \frac{\partial}{\partial Q_j^n} D_{kj}^{mn} \end{aligned} \tag{S38}$$

The first term on the RHS of eq. (S38) would vanish upon integration due to the Gauss divergence theorem, and is not treated further. The second term, upon simplification, may be written as

$$\begin{aligned} \Psi D_{kj}^{mn} \frac{\partial}{\partial Q_j^n} \left[\frac{Q_k^\mu Q_k^\omega Q_k^m}{Q_k^2} \right] = \frac{\delta_{jk} \Psi}{Q_k^4} \Bigg[Q_k^2 \left(D_{kj}^{mn} Q_k^\mu Q_k^\omega \delta^{mn} + D_{kj}^{mn} Q_k^\mu Q_k^m \delta^{n\omega} + D_{kj}^{mn} Q_k^\omega Q_k^m \delta^{n\mu} \right) \\ - 2 D_{kj}^{mn} Q_k^\mu Q_k^\omega Q_k^m Q_k^n \Bigg] \end{aligned} \tag{S39}$$

Noting that

$$\begin{aligned} \sum_{\mu,\omega} \sum_{m,n} D_{kj}^{mn} Q_k^\mu Q_k^\omega \delta^{mn} \boldsymbol{e}_\mu \boldsymbol{e}_\omega &= \mathrm{tr} \left(\boldsymbol{D}_{kj} \right) \boldsymbol{Q}_k \boldsymbol{Q}_k \\ \sum_{\mu,\omega} \sum_{m,n} D_{kj}^{mn} Q_k^\mu Q_k^m \delta^{n\omega} \boldsymbol{e}_\mu \boldsymbol{e}_\omega &= \left(\boldsymbol{Q}_k \boldsymbol{Q}_k \right) \cdot \boldsymbol{D}_{kj} \\ \sum_{\mu,\omega} D_{kj}^{mn} Q_k^\omega Q_k^m \delta^{n\mu} \boldsymbol{e}_\mu \boldsymbol{e}_\omega &= \boldsymbol{D}_{kj}^T \cdot \left(\boldsymbol{Q}_k \boldsymbol{Q}_k \right), \end{aligned} \tag{S40}$$

we may write

$$\left[\sum_{\mu,\omega}\sum_{m,n}\int \Psi D_{kj}^{mn}\frac{\partial}{\partial Q_j^n}\left[\frac{Q_k^\mu Q_k^\omega Q_k^m}{Q_k^2}\right]d\boldsymbol{\mathcal{Q}}\right]\boldsymbol{e}_\mu\boldsymbol{e}_\omega = \left\langle \mathrm{tr}\left(\boldsymbol{D}_{kk}\right)\frac{\boldsymbol{Q}_k\boldsymbol{Q}_k}{Q_k^2}\right\rangle + \left\langle \frac{\boldsymbol{Q}_k\boldsymbol{Q}_k}{Q_k^2}\cdot\boldsymbol{D}_{kk}\right\rangle + \left\langle \boldsymbol{D}_{kk}\cdot\frac{\boldsymbol{Q}_k\boldsymbol{Q}_k}{Q_k^2}\right\rangle - 2\left\langle \boldsymbol{D}_{kk}:\frac{\boldsymbol{Q}_k\boldsymbol{Q}_k\boldsymbol{Q}_k\boldsymbol{Q}_k}{Q_k^4}\right\rangle \tag{S41}$$

where we have used the fact that $\boldsymbol{D}_{kk}$ is a symmetric matrix upon inference from the empirically observed symmetricity of the block diffusion matrix $\boldsymbol{\mathcal{D}}$ [see Fig. S1 and associated discussion].

Furthermore,

$$\left[\sum_{\mu,\omega}\sum_{m,n}\int \Psi\left(\frac{Q_k^\mu Q_k^\omega Q_k^m}{Q_k^2}\right)\frac{\partial}{\partial Q_j^n}D_{kj}^{mn}d\boldsymbol{\mathcal{Q}}\right]\boldsymbol{e}_\mu\boldsymbol{e}_\omega = \left\langle\left(\frac{\boldsymbol{Q}_k\boldsymbol{Q}_k}{Q_k^2}\right)\boldsymbol{Q}_k\cdot\left[\frac{\partial}{\partial\boldsymbol{Q}_j}\cdot\boldsymbol{D}_{kj}^T\right]\right\rangle \tag{S42}$$

From eqs. (S38), (S41), and (S42), we have

$$\left\langle\left(\frac{\boldsymbol{Q}_k\boldsymbol{Q}_k\boldsymbol{Q}_k}{Q_k^2}\right)\cdot\boldsymbol{D}_{kj}\cdot\left(\frac{\partial\ln\Psi}{\partial\boldsymbol{Q}_j}\right)\right\rangle = -\left\langle\left[\mathrm{tr}\left(\boldsymbol{D}_{kk}\right)-2\boldsymbol{D}_{kk}:\frac{\boldsymbol{Q}_k\boldsymbol{Q}_k}{Q_k^2}\right]\frac{\boldsymbol{Q}_k\boldsymbol{Q}_k}{Q_k^2}\right\rangle + \left\langle\frac{\boldsymbol{Q}_k\boldsymbol{Q}_k}{Q_k^2}\cdot\boldsymbol{D}_{kk}\right\rangle + \left\langle\boldsymbol{D}_{kk}\cdot\frac{\boldsymbol{Q}_k\boldsymbol{Q}_k}{Q_k^2}\right\rangle - \left\langle\left(\frac{\boldsymbol{Q}_k\boldsymbol{Q}_k}{Q_k^2}\right)\boldsymbol{Q}_k\cdot\left[\frac{\partial}{\partial\boldsymbol{Q}_j}\cdot\boldsymbol{D}_{kj}^T\right]\right\rangle \tag{S43}$$

The ensemble average in the third term on the RHS of eq. (S33) is simplified as follows

$$\left\langle\left(\frac{\boldsymbol{Q}_k\boldsymbol{Q}_k\boldsymbol{Q}_k}{Q_k^2}\right)\cdot\boldsymbol{M}_{kj}\cdot\left(\boldsymbol{\kappa}\cdot\boldsymbol{Q}_j\right)\right\rangle = \left\langle\left(\boldsymbol{M}_{kj}\cdot\boldsymbol{\kappa}\right)^T:\left[\frac{\boldsymbol{Q}_k\boldsymbol{Q}_j\boldsymbol{Q}_k\boldsymbol{Q}_k}{Q_k^2}\right]\right\rangle \tag{S44}$$

The ensemble average in the last term on the RHS of eq. (S33) may be rewritten as follows

$$\left\langle\left(\frac{\boldsymbol{Q}_k\boldsymbol{Q}_k\boldsymbol{Q}_k}{Q_k^2}\right)\cdot\boldsymbol{D}_{kj}\cdot\boldsymbol{F}_j^{(\mathrm{c})}\right\rangle = \left\langle\left(\frac{\boldsymbol{Q}_k\boldsymbol{Q}_k}{Q_k^2}\right)\left[\boldsymbol{D}_{kj}^T\cdot\boldsymbol{Q}_k\right]\cdot\boldsymbol{F}_j^{(\mathrm{c})}\right\rangle = \left\langle\left[\boldsymbol{D}_{kj}:\boldsymbol{Q}_k\boldsymbol{F}_j^{(\mathrm{c})}\right]\frac{\boldsymbol{Q}_k\boldsymbol{Q}_k}{Q_k^2}\right\rangle \tag{S45}$$

Substituting eqs. (S44) and (S45) into eq. (S33), and plugging the resulting expression into eq. (S18), the dimensional stress tensor expression is obtained as

$$\begin{aligned}\boldsymbol{\tau}_{\mathrm{p}} = {}& n_{\mathrm{p}}k_BT\boldsymbol{\delta} - n_{\mathrm{p}}\sum_{k=1}^{N}\left\langle\boldsymbol{Q}_k\boldsymbol{F}_k^{(\mathrm{c})}\right\rangle - n_{\mathrm{p}}K\sum_{k,j=1}^{N}\left\langle\left(\boldsymbol{M}_{kj}\cdot\boldsymbol{\kappa}\right)^T:\left[\frac{\boldsymbol{Q}_k\boldsymbol{Q}_j\boldsymbol{Q}_k\boldsymbol{Q}_k}{Q_k^2}\right]\right\rangle \\ & + \frac{2n_{\mathrm{p}}k_BTK}{\zeta}\sum_{k,j=1}^{N}\left[\left\langle\frac{\boldsymbol{Q}_k\boldsymbol{Q}_k}{Q_k^2}\cdot\boldsymbol{D}_{kk}\right\rangle + \left\langle\boldsymbol{D}_{kk}\cdot\frac{\boldsymbol{Q}_k\boldsymbol{Q}_k}{Q_k^2}\right\rangle - \left\langle\left(\frac{\boldsymbol{Q}_k\boldsymbol{Q}_k}{Q_k^2}\right)\boldsymbol{Q}_k\cdot\left[\frac{\partial}{\partial\boldsymbol{Q}_j}\cdot\boldsymbol{D}_{kj}^T\right]\right\rangle\right. \\ & \left. - \left\langle\left[\mathrm{tr}\left(\boldsymbol{D}_{kk}\right)-2\boldsymbol{D}_{kk}:\frac{\boldsymbol{Q}_k\boldsymbol{Q}_k}{Q_k^2}\right]\frac{\boldsymbol{Q}_k\boldsymbol{Q}_k}{Q_k^2}\right\rangle\right] + \frac{2n_{\mathrm{p}}K}{\zeta}\sum_{k,j=1}^{N}\left\langle\left[\boldsymbol{D}_{kj}:\boldsymbol{Q}_k\boldsymbol{F}_j^{(\mathrm{c})}\right]\frac{\boldsymbol{Q}_k\boldsymbol{Q}_k}{Q_k^2}\right\rangle\end{aligned} \tag{S46}$$

The dimensionless form of eq. (S46) is given by eq. (39) in the main text.

REFERENCES

[1]R. Kailasham, R. Chakrabarti, and J. R. Prakash, J. Chem. Phys. **149**, 094903 (2018).
[2]R. Kailasham, R. Chakrabarti, and J. R. Prakash, J. Rheol. **65**, 903 (2021).
[3]W. Press, S. Teukolsky, W. Vetterling, and B. Flannery, *Numerical Recipes 3rd Edition: The Art of Scientific Computing* (Cambridge University Press, 2007).
[4]R. B. Bird, C. F. Curtiss, R. C. Armstrong, and O. Hassager, *Dynamics of Polymeric Liquids - Volume 2 : Kinetic Theory* (John Wiley and Sons, New York, 1987).
[5]N. J. Wagner and H. C. Öttinger, J. Rheol. **41**, 757 (1997).
[6]J. R. Prakash, in *Rheology Series*, Vol. 8, edited by D. A. Siginer, D. De Kee, and R. P. Chhabra (Elsevier, 1999) pp. 467–517.